LOW FIELD TRANSPORT PROPERTIES OF A GaAs/$Ga_{1-x}Al_xAs$ SUPERLATTICE

by

Graham James Warren

A thesis submitted for
the degree of Doctor of Philosophy.
Department of Physics,
University of Warwick.
September 1988

ACKNOWLEDGEMENTS

I would like to thank all the members of staff at the physics department of Warwick University for all help received and for making my stay there a pleasent one. I would like to pay special thanks to my supervisor Prof. P.N.Butcher for all the help, encouragement and advice that he gave to me. His enthusiasm for and knowledge of physics made working for him a pleasure. I would also like to thank my fellow PhD. students, especially Dr. Phil Milsom, who taught me many things, including some physics, and Dave Holton for being such a good friend. Finally, I would like to thank my parents for all encouragement and support given.

Papers and Conferences

Part of chapter four was published in Semiconductor Science and Technology. **1**, 2, 133, co-authored by Prof. P.N.Butcher.

This work was also presented as a talk at the IOP solid state conference at Reading, December 1986.

Part of chapter five was presented as a poster at the IOP solid state conference at Imperial College, London, December 1987.

ABSTRACT

This thesis presents some low field mobility, thermopower and Hall factor results for a $GaAs/Ga_{1-x}Al_xAs$ superlattice. For these calculations, acoustic phonon scattering and polar optic phonon scattering are considered. For the acoustic phonon calculation, the zero magnetic field Boltzmann equation is solved using the relaxation time approximation to give the mobility and thermopower results. The thermopower results show a positive peak which is a direct consequence of the small scale of the structure of the superlattice. The polar optic phonon results are obtained using both the relaxation time approximation, which is not strictly valid in this case, and also by an exact numerical iterative method. This shows the relaxation time mobility results to be less than the exact numerical solution by up to a factor of about two. This is due to the inelasticity of the scattering mechanism and the anisotropic nature of the miniband structure.

The Hall factors are calculated using a novel method. Using this method, it is not necessary to solve the non-zero magnetic field Boltzmann equation. Instead, the zero magnetic field Boltzmann equation is solved for two perpendicular orientations of applied electric field, and these zero magnetic field distribution functions are then used to simply calculate the Hall factors. The deviations of the resulting Hall factors from one can give direct information about the form of the miniband structure. Some simple analytical calculations are used to complement the numerical results.

CONTENTS

CHAPTER 1

Introduction

1.1 . Scope

The aim of this thesis is to calculate some of the basic transport coefficients for a new type of semiconductor system, a $GaAs/Ga_{1-x}Al_xAs$ superlattice.

The superlattice structure was first devised about twenty years ago (Esaki and Tsu, 1970), and is simply a periodic structure made by growing ultrathin layers of two different semiconducting materials alternately on top of eachother. By altering the thickness, composition or doping of the layers, many properties of the resulting structure can be tailored. This thesis describes a superlattice with the two types of layers being composed of $GaAs$ and $Ga_{1-x}Al_xAs$. The development of the physics of superlattice systems and related structures such as quantum wells is charted in the next section of this chapter.

The second chapter briefly explores the large field of transport theory in the solid state and describes the chosen method of calculating the transport parameters here, an exact numerical calculation, along with the method that is most commonly used in theoretical calculations, the relaxation time approximation. This transport theory is made relevant to superlattice systems by including a simple band structure calculation of a $GaAs/Ga_{1-x}Al_xAs$ superlattice and a discussion on how the resulting highly anisotropic minibands will affect the choice of method used for the transport calculation.

In chapter three, some results are presented for a superlattice when the electron transport is parallel to the layers of the superlattice and when there is no applied magnetic field present.

The electron mobility is calculated with the system under various conditions using the two methods and a comparison is made between the two. Some

significant differences are observed. In the later sections of chapter three some thermopower results are presented and discussed.

The layout of chapter four is very similar to chapter three, except that, for this chapter, the transport is through the superlattice layers, in the growth direction. Transport in this orientation is commonly called vertical transport. Some different and interesting results are seen in this chapter, and the effect of the superlattice structure is more prominent.

In chapter five, some transport properties are calculated when a small magnetic field is applied to the system. The method used to calculate the Hall factors is a novel one and it involves little extra work to obtain the Hall factors if the mobility calculations have been previously carried out. The numerical calculations of this chapter are then compared with some analytical results when some simplifying approximations are made.

Finally, the conclusions to the thesis are drawn in chapter six.

1.2 . Low Dimensional Structures

Low dimensional structures are systems where the length scale of some property of the system in one or more direction is small enough to radically alter the physical processes from those observed in the bulk. The large current interest in these systems has arisen due to the good quality of interfaces produced by the modern growth techniques of molecular beam epitaxy (MBE) (Cho and Arthur, 1975; Ploog, 1980) and metalorganic vapour phase epitaxy (MOVPE) (Dapkus, 1984). It is important that the interfaces in these structures be free from defects so that disorder effects and localised surface states do not hide the interesting properties due to the small scale of the structure.

There are several types of low dimensional structures, with one, two or many interfaces. With one interface a single heterojunction is formed, such as the GaAs/(AlGa)As heterojunction (Tsui and Logan, 1979; Störmer et al, 1979), and the electrons form a 2-dimensional electron gas (2DEG) in an inversion layer at the interface. Another way of forming a 2DEG is with two interfaces close together giving a structure such as the (AlGa)As/GaAs/(AlGa)As single quantum well. The conduction band is lower in energy in the central material and so the central layer acts as a potential well, confining the electrons in one of the dimensions. This confinement, in the quantum well or the heterojunction, produces descrete electron energy levels, onto which is superimposed the dispersion for movement in the other two dimensions, and 'sub-bands' are formed. The properties of systems where 2DEG's are formed has been excellently reviewed (Ando, Fowler and Stern, 1982).

The next class of structures is that of semiconductor superlattices, in which there is a periodic array of interfaces between two materials. This is the structure studied in this thesis. The superlattice was first proposed in 1970 (Esaki and Tsu, 1970) and the report of the first successful growth of a superlattice was three years later (Chang et al, 1973). Since then there has been much work on superlattice structures which is described in several

good review articles (Ploog and Döhler, 1983; Esaki, 1984; Kelly and Nicholas, 1985). The interest in superlattices arose from the possibility of observing Bloch oscillations due to the reduced size in the growth direction (Esaki and Tsu, 1970). This would result in the current voltage curve displaying negative differential resistance (NDR), which is of use in device applications. Also, further interest is due to the ability to tailor the electronic and spatial properties of the system (Esaki and Chang, 1976). More recently, due to the very high mobilities possible, $> 10^6 cm^2 V^{-1} s^{-1}$, where the electrons have ballistic behaviour over distances of $\sim 10 \mu m$, the possibility of vacuum valve physics on a micron scale is being studied (Störmer, 1983). A summary of the implications of LDS for electronic devices by Hess and Iafrate shows the possible future importance of these structures (Hess and Iafrate, 1984).

Figure 1.1 shows the superlattice potential seen by the electrons of mass $m^*(z)$ within the effective mass theory, ie. it is the potential inserted into the effective mass Hamiltonian.

$$-\frac{\hbar}{2}\nabla\cdot\left(\frac{1}{m^*(z)}\nabla\right)F + V_{SL}(z)F = EF \tag{1.1}$$

The effective mass here is now a function of position, having a different value in the two semiconducting materials. This Hamiltonian is discussed further in chapter 2.

There are several different types of superlattices depending on the composition of the layers. The superlattice studied in this thesis, a GaAs/(AlGa)As superlattice, is a type I superlattice. In a type I superlattice, the potential well for both the electrons and the holes is formed in one of the materials, in this case in the GaAs layers. $GaAs$ and $Ga_{1-x}Al_xAs$ is the most widely studied combination of layer materials, largely due to the similarity in the lattice constants of the two materials. Any mismatch in the lattice constants will produce strains at the interfaces which will make the growth of abrupt interfaces more

difficult. However, strained layer superlattices, such as Si/(SiGe) superlattices, have gained considerable interest recently (Voisin, 1984; Abstreiter et al, 1984).

In a type II superlattice (Sai-Halasz et al, 1977), the potential well for the electrons is not in the same material as the hole potential well, and the electrons and holes are separated in real space. An example of a type II superlattice is the $Ga_xIn_{1-x}As/GaAs_ySb_{1-y}$ structure (Sakaki et al, 1977), with the $Ga_xIn_{1-x}As$ forming the well for the electrons and the $GaAs_ySb_{1-y}$ forming the well for the holes.

The idea of an 'effective mass' superlattice has also been proposed (Sasaki, 1984), where there is no discontinuity in the conduction bands of the two materials, but where the an electron has a different effective mass in the alternating layers. Some possible materials to achieve this were proposed by Sasaki.

A final design parameter of a superlattice that must be mentioned is the doping. With the modern growth techniques used, it is possible to selectively dope the different layers in different ways, producing modulation doped structures (Dingle et al, 1978). One possible advantage of this technique is that, if only the barrier material is doped, a real space separation of the ionised impurities and the charge carriers is achieved, and the scattering is reduced.

The electrons in a superlattice, in the absence of strong disorder (either interface roughness or alloy disorder), are no longer localised in one dimension to form a 2DEG, but have wavefunctions extended throughout the system. This is because the periodicity of the system is retained and Bloch's theorem still applies. Instead of forming discrete energy levels due to the structure in the growth direction, 'minibands' are formed. If, however, the barrier layers are made very thick, the minibands become very narrow and only a very small amount of disorder is needed to localise the electrons. In this case, it is more appropriate to treat the superlattice as an array of 2DEG's, with phonon activated hopping between the layers (Calecki et al, 1984).

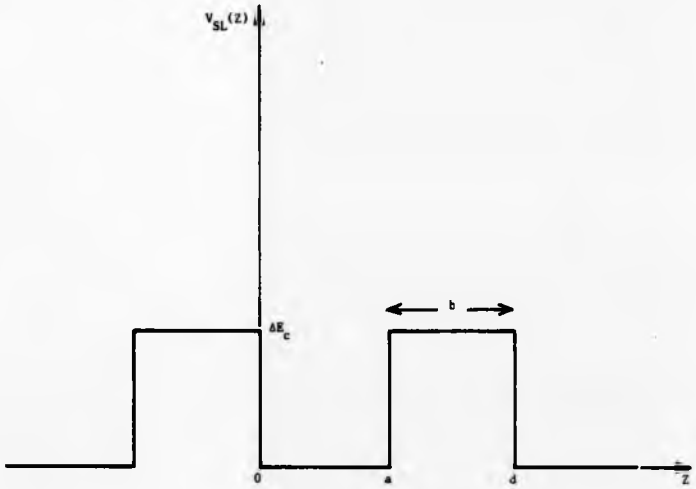

Figure 1.1: The effective potential for a superlattice with well width a and barrier width b.

PAGINATION
ERROR

CHAPTER 2

Transport Theory

In this chapter, the foundations needed for a calculation of the transport properties of a GaAs/GaAlAs superlattice are introduced. We start off with a discussion of the band structure of the system and an overview of the methods used to evaluate the miniband dispersion relation. This is followed by a brief examination of the transport equations and a look at the methods used for solving the Boltzmann transport equation (B.T.E.). Finally, the scattering mechanisms considered are discussed at the end of the chapter.

2.1 . Miniband Structure

Many of the interesting properties of a superlattice are a consequence of its highly anisotropic band structure, and before we can examine the transport properties this band structure must be calculated. To do this we follow Bastard's envelope function approach (Bastard, 1981, 1982), which is based on Kane's $\mathbf{k}\cdot\mathbf{p}$ Hamiltonian (Kane, 1957). The wavefunction is expressed as

$$\psi^{A,B}(\mathbf{r}) = \sum_j F_j^{A,B}(\mathbf{r}) U_{j_0}^{A,B}(\mathbf{r}) \tag{2.1}$$

where the $F_j^{A,B}(\mathbf{r})$ are slowly varying envelope functions and the $U_{j_0}^{A,B}$ are the periodic part of the Bloch function at the bottom of band j for materials A and B. The Schrödinger equation can be reduced to a 2×2 matrix equation in S and P type envelope functions in the conduction band, $F_{1,2}$.

The details of the calculation are in the original references (Bastard, 1981; Kane, 1957), the important result being that, in place of $F_{1,2}$ and $(dF_{1,2}/dz)$

being continuous, we have that

$$\frac{1}{\epsilon_G + \lambda - V(z)} \left(-\sqrt{2}\frac{dF_1}{dz} - ik_+ F_2 \right) \tag{2.2a}$$

and

$$\frac{1}{\epsilon_G + \lambda - V(z)} \left(-\sqrt{2}\frac{dF_2}{dz} + ik_- F_1 \right) \tag{2.2b}$$

are now continuous. Here, ϵ_G is the band gap in each layer, λ is the electron energy, V(z) is the superlattice potential and $k_\pm = (k_z \pm ik_y)/\sqrt{2}$. For GaAs and GaAlAs, which are wide gap materials, the approximation is made that ϵ_G dominates the denominator of expressions (2.2), and so, if we also assume that the envelope functions are continuous at the interface, then the condition on the derivative at an interface is;

$$\frac{1}{\epsilon_{GaAs}} \frac{dF^{GaAs}}{dz} = \frac{1}{\epsilon_{GaAlAs}} \frac{dF^{GaAlAs}}{dz} \tag{2.3}$$

In Kane's k · p perturbation approach, the conduction band is parabolic for small k values, with the effective mass proportional to the energy gap at k = 0. We therefore have that the continuity equations can be written as,

$$\frac{1}{m^*_{GaAs}} \frac{dF^{GaAs}}{dz} = \frac{1}{m^*_{GaAlAs}} \frac{dF^{GaAlAs}}{dz} \tag{2.4}$$

This continuity relation can be arrived at more simply by treating the electrons as particles with variable mass $m^*(z)$ moving through the superlattice potential V(z). According to Schrödinger's original papers (Schrödinger, 1926; Enders, 1987), a more general form of the Schrödinger equation is, in one dimension,

$$-\frac{\hbar^2}{2} \frac{f(z)}{m^{*1/2}} \frac{d}{dz} \left(\frac{1}{f(z) m^{*1/2}} \frac{dF}{dz} \right) + V(z)F = EF \tag{2.5}$$

where f(z) is an arbitrary function of z. To make the Hamiltonian hermitian

when the mass is a function of z, letting $f(z) = \sqrt{m^*(z)}$ gives

$$H = -\frac{\hbar^2}{2}\frac{d}{dz}\left(\frac{1}{m^*(z)}\frac{d}{dz}\right) + V(z) \tag{2.6}$$

Now, starting from this Hamiltonian it is simple to derive the previous continuity relation by integrating it across a narrow interface. This Hamiltonian also produces the necessary result that the current density is continuous across an interface.

The effective mass theory using the continuity relation (2.4) is also in agreement with a first principles calculation of Marsh and Inkson (Marsh and Inkson, 1984), whereas the usual continuous derivative condition does not agree (Collins et al, 1985).

Now, using this condition along with Bloch's theorem,

$$F(z + md) = e^{ik_z md}F(z) \tag{2.7}$$

where m is an integer, d is the superlattice period and k_z is the electron wavevector in the z-direction, the dispersion relation is simply derived, for $k_{\|} = 0$, as (Bastard, 1981),

$$\cos k_z d = \cos k_z a \cos k_b b - 1/2\left(\frac{m_b^* k_a}{m_a^* k_b} + \frac{m_a^* k_b}{m_b^* k_a}\right)\sin k_z a \sin k_b b \tag{2.8}$$

where

$$k_a^2 \equiv \frac{2m_a^*}{\hbar^2}\epsilon_z \tag{2.9a}$$

$$k_b^2 \equiv \frac{2m_b^*}{\hbar^2}(\epsilon_z - V_S) \tag{2.9b}$$

ϵ_z is the electron energy due to motion in the z-direction, V_S is the conduction band discontinuity and a,b are respectively the well and barrier region widths.

The value of V_S, along with m^*, is taken from a paper of Okumara et al (1985), and, as a function of the alloy concentration x are $V_S = 0.67\Delta E_g = 831x$ meV and $m^* = (0.067+0.083x)m_0$, where ΔE_g is the bandgap difference between GaAs and the alloy, and m_0 is the free electron mass.

For the bandstructure in the $k_\parallel$ direction, we make the frequently used approximation (Artaki & Hess, 1985; Movaghar, 1986; Lobwohl and Tsu, 1970), and say that the band is parabolic with an effective mass averaged over the layers.

$$\epsilon_\parallel = \frac{\hbar^2 k_\parallel^2}{2m^*} \tag{2.10}$$

where

$$m^* = (am_a^* + bm_b^*)/d \tag{2.11}$$

Now, we could use this bandstructure for the transport problems, but it is clumsy and so we replace it with a simple phenomenological form

$$\epsilon = \frac{\hbar^2 k_\parallel^2}{2m^*} + \Delta(1 - \cos k_z d) \tag{2.12}$$

where 2Δ is the miniband width, and is obtained from the previous calculation. The phenomenological bandstructure is compared with the Kronig-Penny calculation in figure 2.1.

The density of states for the phenomenological bandstructure is shown in figure 2.2. The DOS rises rapidly as the energy moves up through the miniband, and then exhibits 2D like behaviour and becomes constant between minibands.

There are several sophisticated calculations of the band structure (Wong et al, 1986; Ivanov and Pollmann, 1979; Ting and Chang, 1987; Marsh and Inkson, 1984), but to use them in a transport calculation would be difficult. The simple form that is used here has the essential feature that it is highly anisotropic and so will show the features in the results that are peculiar to the superlattice structure.

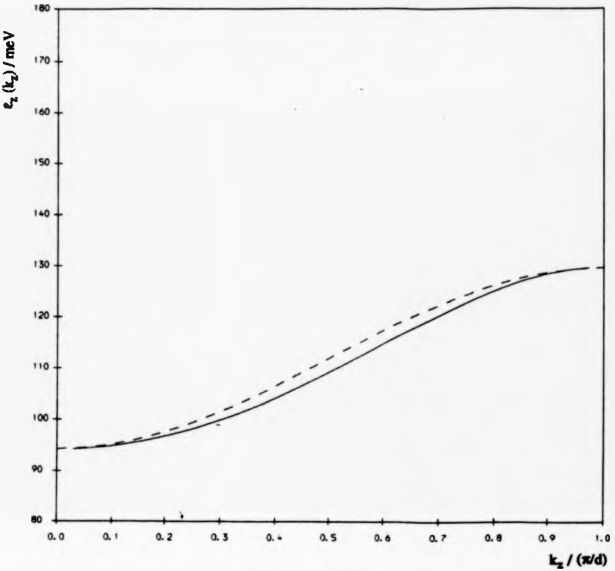

Figure 2.1: The miniband structure of a GaAs/$Ga_{1-x}Al_xAs$ superlattice with a period of 70Å and an alloy concentration of x=0.3. The full curve is the Kronig-Penny calculation and the dashed curve is the phenomenological form, $\varepsilon=\Delta(1-\cos(k_z d))$.

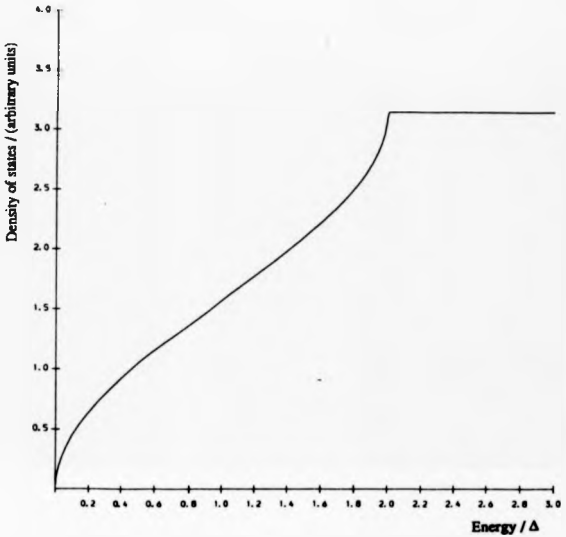

Figure 2.2: The density of states for a superlattice with the phenomenological band structure $\varepsilon=\Delta(1-\cos(k_z d))$.

2.2 . Transport Theory

2.2.1 . Introduction

In this section the ideas and methods for examining the transport properties of a solid state system are introduced. The requirement is to have a method of approach that gives a physical feel for the processes involved in the conduction of charge or heat, is simpler to use than a full quantum mechanical treatment and yet is sufficiently accurate. This is achieved by developing a semi-classical description of the dynamics of the electrons when force fields are applied. Starting from this simplified model, a semi-classical transport equation, the Boltzmann equation, is derived and some methods for solving this equation to calculate the perturbed electron distribution function in (**k**,**r**) space are discussed.

The first is the relaxation time approximation, which gives a physically intuitive solution to the problem but is inaccurate in some situations, specifically when the scattering mechanism involved is inelastic and when the band structure is not spherically symmetric, which is the case for a superlattice.

The second method is the more direct iterative solution of Rode (Rode, 1970, 1975) which gives an exact numerical solution of the Boltzmann equation.

Once the electron distribution function, f(**k**,**r**), has been found, all the transport coefficients can be calculated very simply.

In this chapter, only electric fields are considered in detail, with the situation with magnetic fields present being discussed fully in chapter five.

The scattering mechanisms that are considered are acoustic phonon scattering, which is quasi-elastic at high temperatures and may be treated with the relaxation time approximation, and polar optic phonon scattering, which is highly inelastic and must be treated with Rode's iterative method.

2.2.2 . Transport Coefficients

To characterize how a system responds to the application of electric and magnetic fields, and temperature gradients, the following relationships are defined (Butcher, 1973).

$$\mathbf{J} = \sigma \mathbf{E}' + L \nabla T \tag{2.13a}$$

$$\mathbf{Q} = M \mathbf{E}' + N \nabla T \tag{2.13b}$$

which determines the current density $\mathbf{J}$ and the heat current $\mathbf{Q}$ with an electromotive force and a temperature gradient ∇T applied. The electromotive force is given in terms of the applied electric field $\mathbf{E}$ and chemical potential μ as,

$$\mathbf{E}' = \mathbf{E} + \frac{1}{e} \nabla \mu \tag{2.14}$$

It is more usual for equation (2.13) to be inverted to give,

$$\mathbf{E}' = \rho \mathbf{J} + S \nabla T \tag{2.15a}$$

$$\mathbf{Q} = \pi \mathbf{J} - \kappa \nabla T \tag{2.15b}$$

where ρ is the resistivity, $\mathbf{S}$ is the thermoelectric power, π is the peltier coefficient and κ is the thermal conductivity. In general, these coefficients are second rank tensors and depend on the applied magnetic field.

The conductivity (and the other transport coefficients) can be written in the following power series form to include the effects of a weak magnetic field.

$$\sigma_{ij}(\mathbf{B}) = \sigma_{ij}(0) + \frac{\partial \sigma_{ij}(0)}{\partial B_k} B_k + \frac{1}{2} \frac{\partial^2 \sigma_{ij}(0)}{\partial B_k \partial B_l} B_k B_l + \ldots \tag{2.16}$$

and so, to first order in $\mathbf{B}$, the current density $\mathbf{J}$, with zero temperature

gradient, is given by,

$$J_i = \sigma_{ij} E_j + C_{ijk} E_j B_k \tag{2.17}$$

where $\sigma_{ij} = \sigma_{ij}(0)$ and $C_{ijk} = \frac{\partial \sigma_{ij}(0)}{\partial B_k}$. Repeated indices are summed over.

The symmetry properties of these tensors for the case of tetragonal symmetry of a superlattice is discussed in appendix A.

2.2.3 . The Boltzmann Transport Equation

To derive a semi-classical transport equation, we must describe the motion of our electrons in semi-classical terms. Using effective mass theory (Luttinger & Kohn, 1955; Smith et al, 1967; Stoneham, 1975), the following intuitive equations describing the behaviour of the electron wavepackets can be rigorously derived.

$$\frac{d\mathbf{r}}{dt} = \mathbf{v} = \frac{1}{\hbar} \nabla_k \epsilon(\mathbf{k}) \tag{2.18a}$$

$$\hbar \frac{d\mathbf{k}}{dt} = -e[\mathbf{E} + \mathbf{v} \times \mathbf{B}] \tag{2.18b}$$

Thus, we have assigned a position **r** and a wavevector **k** to the electron wavepacket, and have the equations of motion that determine the time variation of **r** and **k** with electric and magnetic fields present.

In a crystalline material, there is a large number of electrons present, and so it is necessary to describe them by a distribution function in the six dimensional (**k**,**r**) space, f(**k**,**r**,t), which is defined as the probability that an electron will be found in the state $|\mathbf{k}>$ in the neighbourhood of the point **r** at a time t. Since spin does not enter into the calculation, the density of electrons in (**k**,**r**) space per unit volume is $\frac{1}{4\pi^3} f(\mathbf{k},\mathbf{r},t)$.

In thermal equilibrium at temperature T with no external fields, statistical mechanics for fermions tells us that the distribution function is the Fermi-Dirac distribution function

$$f_0(\mathbf{k}) = \frac{1}{\exp\{\beta[\epsilon(\mathbf{k}) - \mu]\} + 1} \tag{2.19}$$

where $\beta \equiv (k_B T)^{-1}$, k_B is the Boltzmann constant and μ is the chemical potential.

To calculate the distribution function with fields present, we use the Boltzmann equation,

$$\frac{\partial f}{\partial t} + \mathbf{v} \cdot \nabla f + \mathbf{F}' \cdot \nabla_k f = \left(\frac{\partial f}{\partial t}\right)_{COLL} \tag{2.20}$$

where $\mathbf{F}' = -\frac{e}{\hbar}[\mathbf{E} + \mathbf{v} \times \mathbf{B}]$.

The second term on the left hand side gives the rate of change in f(k,r,t) due to diffusion in real space, the third term is the drift of electrons in k-space due to the applied fields and $\left(\frac{\partial f}{\partial t}\right)_{COLL}$ is due to the scattering of electrons from phonons, impurities etc.. This collision term can be expressed in terms of scattering rates

$$\left(\frac{\partial f}{\partial t}\right)_{COLL} = \int \{P(\mathbf{k}', \mathbf{k}) f(\mathbf{k}')[1 - f(\mathbf{k})] - P(\mathbf{k}, \mathbf{k}') f(\mathbf{k})[1 - f(\mathbf{k}')]\}\ d\mathbf{k}' \tag{2.21}$$

where $\frac{2\pi}{V} P(\mathbf{k}, \mathbf{k}')$ is the scattering rate from state $|\mathbf{k}>$ to state $|\mathbf{k}'>$.

To proceed in the case when the applied electric field is small and there is no magnetic field present, we write

$$f(\mathbf{k}) = f_0(\mathbf{k}) + g(\mathbf{k}) \tag{2.22}$$

where $\mathbf{g(k)}$ is a small perturbation to the distribution function. We now linearize the BTE, ignoring terms of second order in $\mathbf{g(k)}$. This gives us, for a steady state problem (Butcher,1973)

$$-\frac{e}{\hbar}\mathbf{E} \cdot \nabla_k f_0 = \left(\frac{\partial g}{\partial t}\right)_{COLL} \tag{2.23}$$

where

$$\left(\frac{\partial g}{\partial t}\right)_{COLL} = \int \{g(\mathbf{k}')[(1 - f_0(\mathbf{k}))P(\mathbf{k}', \mathbf{k}) + f_0(\mathbf{k})P(\mathbf{k}, \mathbf{k}')]$$

$$- g(\mathbf{k})[f_0(\mathbf{k}')P(\mathbf{k}', \mathbf{k}) + (1 - f_0(\mathbf{k}'))P(\mathbf{k}, \mathbf{k}')]\}\ d\mathbf{k}' \quad (2.24)$$

This is the equation that we set out to solve in chapters 3-5.

2.2.4 . The Relaxation Time Approximation

The first method of approach to the solution of equation (2.23) has always been the relaxation time approximation which makes the assumption that

$$\left(\frac{\partial g}{\partial t}\right)_{COLL} = -\frac{g(\mathbf{k})}{\tau} \quad (2.25)$$

where τ is the relaxation time. However, this approach is invalid for the GaAs/GaAlAs superlattice system. It can be shown (Butcher,1973) that for the relaxation time approximation to be exact, the bands must be spherical and the scattering mechanism must be either elastic or velocity randomizing $[P(\mathbf{k}, \mathbf{k}') = P(\mathbf{k}, -\mathbf{k}')]$. The GaAs/GaAlAs superlattice bandstructure is highly anisotropic, which will lead to a breakdown of the relaxation time approximation. Also, at high temperatures, the dominant scattering mechanism in GaAs, a strongly polar material, is polar optic phonon scattering, which is highly inelastic and is not velocity randomizing (Ehrenreich, 1961). Thus, a different method must be used to obtain more accurate results for the superlattice transport properties.

2.2.5 . The Iterative Method

When the relaxation time approximation is not adequate, the method used is an iterative technique based on an algorithm developed by Rode (Rode, 1970). From equations (2.23) and (2.24), the linearized Boltzmann equation can be rearranged into the form

$$g(\mathbf{k}) = \frac{\int\{g(\mathbf{k}')[(1-f_0(\mathbf{k}))P(\mathbf{k}',\mathbf{k}) + f_0(\mathbf{k})P(\mathbf{k},\mathbf{k}')]\}\ d\mathbf{k}' + \frac{e}{\hbar}\mathbf{E}\cdot\nabla_k f_0}{\int\{f_0(\mathbf{k}')P(\mathbf{k}',\mathbf{k}) + (1-f_0(\mathbf{k}'))P(\mathbf{k},\mathbf{k}')\}\ d\mathbf{k}'} \tag{2.26}$$

or, if we are specifically dealing with the case of non-degenerate statistics, where $f(\mathbf{k}) \ll 1$, then we may further simplify equation (2.26) to give

$$g(\mathbf{k}) = \frac{\int\{g(\mathbf{k}')P(\mathbf{k}',\mathbf{k})\}\ d\mathbf{k}' + \frac{e}{\hbar}\mathbf{E}\cdot\nabla_k f_0}{\int P(\mathbf{k},\mathbf{k}')\ d\mathbf{k}'} \tag{2.27}$$

Now, equations (2.26) and (2.27) have the required solution $g(\mathbf{k}')$ on the R.H.S., and so a natural approach to their solution is to choose an initial guess for $\mathbf{g(k)}$ and iterate until convergence is obtained. If the initial guess is $\mathbf{g(k)}$=0 for all values of $\mathbf{k}$, then the first iteration gives

$$g_1(\mathbf{k}) = \frac{\frac{e}{\hbar}\mathbf{E}\cdot\nabla_k f_0}{\int P(\mathbf{k},\mathbf{k}')\ d\mathbf{k}'} \tag{2.28}$$

But, the denominator of equation (2.28) is just the reciprocal of the intrinsic lifetime of an electron in state $|\mathbf{k}>$.

$$\frac{1}{\tau(\mathbf{k})} = \int\{P(\mathbf{k},\mathbf{k}')\}\ d\mathbf{k}' \tag{2.29}$$

Thus, the first iteration is the answer that would be obtained using the relaxation time approximation with the relaxation time given by the intrinsic lifetime of the electron state.

The convergence of this procedure has been examined by Rode (Rode, 1975) who concludes that the final solution g_∞ is unique and that the procedure

converges exponentially, so that very few iterations are needed for a reasonable accuracy.

If the electric field is in the growth direction, $\mathbf{E} = (0, 0, E_z)$, then from the symmetry of the problem the perturbation g cannot depend on θ, ie. $g \equiv g(k_{\|}, k_z)$, and we have

$$g(k_{\|}, k_z) = \frac{\int\{g(k'_{\|}, k'_z)[(1 - f_0(\mathbf{k}))P(\mathbf{k}', \mathbf{k}) + f_0(\mathbf{k})P(\mathbf{k}, \mathbf{k}'))]\}\ d\mathbf{k}' + \frac{q}{\hbar}E_z\frac{\partial f_0}{\partial k_z}}{\int\{f_0(\mathbf{k}')P(\mathbf{k}', \mathbf{k}) + (1 - f_0(\mathbf{k}'))P(\mathbf{k}, \mathbf{k}')\}\ d\mathbf{k}'} \tag{2.30}$$

and g can be represented numerically by a two-dimensional array.

If, however, the electric field is in the layers, $\mathbf{E} = (E_z, 0, 0)$, then it can be shown that the θ-dependence is a simply $\cos\theta$ term, and the perturbation is given by (appendix B)

$$\tilde{g}(k_{\|}, k_z) = \frac{\int\{\tilde{g}(k'_{\|}, k'_z)[(1 - f_0(\mathbf{k}))P(\mathbf{k}', \mathbf{k}) + f_0(\mathbf{k})P(\mathbf{k}, \mathbf{k}')]\}\ d\mathbf{k}' + \frac{q}{\hbar}E_z\frac{\partial f_0}{\partial k_z}\frac{k^2 k_{\|}}{m^*}}{\int\{f_0(\mathbf{k}')P(\mathbf{k}', \mathbf{k}) + (1 - f_0(\mathbf{k}'))P(\mathbf{k}, \mathbf{k}')\}\ d\mathbf{k}'} \tag{2.31}$$

with

$$g_z(\mathbf{k}) = \tilde{g}(k_{\|}, k_z)\cos\theta \tag{2.32}$$

The essential difference between the iterative method and the relaxation time approximation is that the relaxation time approximation neglects electron scattering into the volume element $d\mathbf{k}$, whereas they are included in the iterative approach. It will be shown in later chapters that there is a significant difference in the results given by the two methods for polar optic phonon scattering.

2.3 . The Scattering Mechanisms

The main aim of this thesis is to examine the effect of the superlattice structure on the electronic transport properties. To do this we consider the scattering mechanisms that are important in GaAs/GaAlAs systems and treat them simplistically to demonstrate the effect of the anisotropic bandstructure associated with a superlattice. The scattering mechanisms considered are deformation potential acoustic phonon scattering and polar optic phonon scattering, the latter being the dominant mechanism in GaAs at high temperatures.

In these calculations, we mainly consider systems with low electron concentrations and so we treat the electron-phonon interaction as unscreened. Also, the effect of the layer structure on the phonon dispersion relation is not taken into account.

The first scattering mechanism considered is deformation potential scattering by acoustic phonons, with the transition rate given by (Nag, 1972; Bardeen & Shockley, 1950),

$$P_{ac}(\mathbf{k},\mathbf{k}') = \frac{(N_q + 1/2 \pm 1/2)}{8\pi^2\omega\rho} E_1^2 |\mathbf{k}-\mathbf{k}'|^2 \delta(\epsilon(\mathbf{k}') - \epsilon(\mathbf{k}) \pm \hbar\omega(q)) \quad (2.33a)$$

$$= \frac{(N_q + 1/2 \pm 1/2)}{8\pi^2 S^2\rho} E_1^2 \omega \delta(\epsilon(\mathbf{k}') - \epsilon(\mathbf{k}) \pm \hbar\omega(q)) \quad (2.33b)$$

where $N_q = \left(\exp\frac{\hbar\omega(q)}{k_B T} - 1\right)^{-1}$ is the equilibrium phonon distribution, ρ is the material density, E_1 is the deformation potential, ω is the phonon frequency and $S = \omega/q$ is the speed of sound in the material. The (+) and (-) signs refer to phonon emission and absorption respectively. The use of the equilibrium phonon distribution here excludes non-equilibrium effects, such as phonon drag.

Now, except at very low temperatures, this scattering mechanism can be treated as quasi-elastic, as typically $\hbar\omega \ll \epsilon(\mathbf{k})$, which will greatly simplify the transport calculations.

The second scattering mechanism is polar optic phonon scattering, which has the Fröhlich scattering rate (Fröhlich, 1937, 1962),

$$P_{po}(\mathbf{k},\mathbf{k}') = \frac{e^2\omega_0}{8\pi^2\epsilon_0}\left(\frac{1}{\kappa_\infty}-\frac{1}{\kappa_0}\right)\frac{(N_q+1/2\pm 1/2)}{|\mathbf{k}-\mathbf{k}'|^2}\delta(\epsilon(\mathbf{k}')-\epsilon(\mathbf{k})\pm\hbar\omega_0) \qquad (2.34)$$

where κ_∞ and κ_0 are the high frequency and static dielectric constants respectively.

This scattering mechanism is highly inelastic and so cannot be treated by the relaxation time approximation.

The actual form of the scattering rates will be affected by the superlattice structure, which modifies both the electron and phonon wavefunctions. However, as there are few experimental results of the type needed for a detailed comparison with the theory here (for some results, see Palmier and Chomette, 1982), it is sufficient to use the scattering rates given here, in which case the calculation illustrates some of the fundamental effects that the superlattice structure produces.

CHAPTER 3

Parallel transport

3.1 . Introduction

A superlattice structure is highly anisotropic, and so there are two distinct cases to consider when dealing with the transport properties. There is the case when the applied electric field is in the growth direction, called vertical transport, and which is dealt with in the next chapter, and parallel transport where the electric field is in the plane of the layers, which is considered here.

In the plane of the layers, the electron dispersion relation is taken to be free-electron like with an effective mass m^*, and so the properties distinct to the superlattice will not be as evident as in the vertical transport situation, but some interesting features are seen.

Most of the original transport calculations for a superlattice were for parallel transport, with the quantum wells treated as non-interacting (Hess, 1979; Mori and Ando, 1980), so that the electrons are confined in the growth direction and have discrete energy levels associated with this direction.

$$\epsilon(k_{\|}, n) = \epsilon_n + \frac{\hbar^2 k_{\|}^2}{2m^*} \tag{3.1}$$

For wide layers, this is a good approximation, but as the layer thickness becomes small, $d \leq 100\text{Å}$, the discrete energy levels broaden out into minibands with small but significant band widths, seen in figure 3.1, and the dispersion relation (2.12) must be used.

The gaps between the minibands are generally quite large, $\geq 100meV$, and so transitions into higher minibands are not considered here.

For parallel transport, we have $\mathbf{E} = (\mathbf{E}_{\|}, 0)$, where $\mathbf{E}_{\|}$ is a 2D vector in the

plane of the layers, and so the driving term of the BTE is

$$\frac{e}{\hbar}\mathbf{E}\cdot\nabla_k f_0 = \frac{e}{\hbar}E_{\|}\frac{\partial f_0}{\partial k_{\|}}\cos\theta \tag{3.2a}$$

$$= \frac{e}{\hbar}E_{\|}\frac{df_0}{d\varepsilon}\frac{\hbar^2 k_{\|}}{m^*}\cos\theta \tag{3.2b}$$

which can be substituted into equation (2.26).

To proceed further with the mobility calculation, the specific scattering mechanism must be considered.

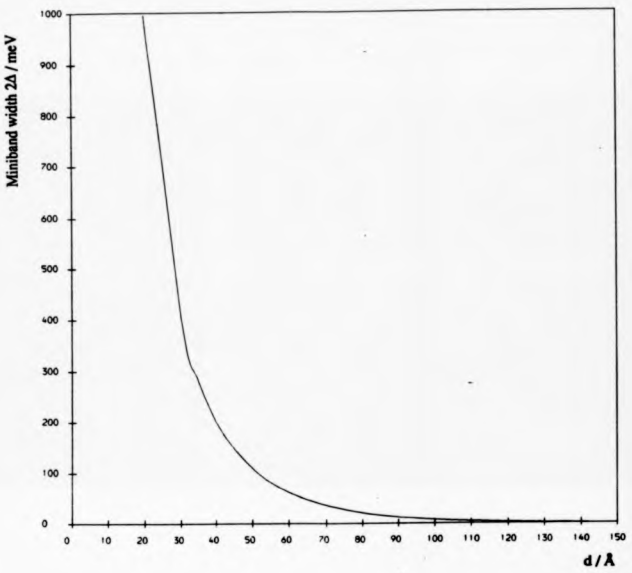

Figure 3.1: A Kronig-Penny calculation of the miniband width 2Δ of a GaAs / $Ga_{1-x}Al_xAs$ superlattice as the period is varied. The alloy concentration is x = 0.3.

3.2 . Mobility

3.2.1 . Acoustic Phonon Scattering

The scattering rate for acoustic phonon deformation potential scattering given by equation (2.33b) is

$$P_{ac}(\mathbf{k},\mathbf{k}') = \frac{(N_q + 1/2 \pm 1/2)\Xi_1^2 q}{\hbar v^2 S^2 \rho}\delta(\epsilon(\mathbf{k}') - \epsilon(\mathbf{k}) \pm \hbar\omega(q)) \tag{3.3}$$

Now, at high temperatures, we can approximate the phonon distribution by,

$$N_q \approx \frac{k_B T}{\hbar\omega} \tag{3.4}$$

whereupon the scattering rate becomes independent of $\mathbf{k}'$ on a constant energy surface. We can treat acoustic phonon deformation potential scattering as quasi-elastic, which is a good approximation because, for semiconductors, we have (Butcher,1971),

$$\hbar\omega = \hbar q S \approx \hbar k S \approx \frac{\epsilon(\mathbf{k})S}{|\mathbf{v}(\mathbf{k})|} \ll \epsilon(\mathbf{k}) \tag{3.5}$$

The last inequality arises because the velocity of sound is much less than a typical electron velocity, except at very low temperatures.

Now, when the electric field is in the plane of the layers, along the x-axis, the perturbation to the distribution function can be written in the form

$$g_x(\mathbf{k}) = \tilde{g}_x(k_{||}, k_z)\cos\theta \tag{3.6}$$

For acoustic phonon scattering, the scattering rate is independent of θ, and so the 'scattering-in' term in the numerator of equation (2.26) can be separated

out to give

$$S_i = \int\int F(k_{\|}, k_z)\ dk_{\|}\ dk_z\ \times \int_0^{2\pi} \cos\theta\ d\theta \tag{3.7}$$

$$=0$$

Thus, the first iteration is the exact solution and the relaxation time approximation holds true.

The relaxation time is, in this case, given by the intrinsic lifetime of an electron in state $|\mathbf{k}>$

$$\frac{1}{\tau_{ac}(\mathbf{k})} = \int P_{ac}(\mathbf{k},\mathbf{k}')\ d\mathbf{k}' \tag{3.8}$$

where the scattering rate $P_{ac}(\mathbf{k},\mathbf{k}')$ includes both emission and absorption processes,

$$P_{ac}(\mathbf{k},\mathbf{k}') = \frac{E_1^2 k_B T}{4\pi^2 S^2 \rho\hbar}\delta(\epsilon(\mathbf{k}) - \epsilon(\mathbf{k}')) \tag{3.9}$$

This gives, after some simple integration (Palmier et al, 1980,1982),

$$\frac{1}{\tau_{ac}(\mathbf{k})} = \frac{E_1^2 m^* k_B T}{\pi S^2 \rho\hbar^3} k_1 \tag{3.10}$$

where k_1 is the limit over which the k_z' integral is performed, and is given by

$$k_1 d = \cos^{-1}\left\{1 - \frac{\epsilon(\mathbf{k})}{\Delta}\right\} \qquad ;\epsilon(\mathbf{k}) < 2\Delta \tag{3.11a}$$

$$=\pi \qquad ;\epsilon(\mathbf{k}) \geq 2\Delta \tag{3.11b}$$

With the relaxation time found, we can then simply obtain the distribution function, and thus all the zero magnetic field coefficients.

As we have seen, a relaxation time can be found analytically for acoustic phonon deformation potential scattering and, although acoustic phonons do not play a major part in limiting transport in GaAs compared to polar optic phonon scattering at high temperatures, we will nevertheless show the results here to

illustrate the calculation.

When the electric field is applied in the x-direction, the perturbation to the distribution function can be written down immediately in the relaxation time approximation:

$$g_z(\mathbf{k}) = \frac{e}{\hbar} E_{\|} \frac{df_0}{d\epsilon} \frac{\hbar^2 k_{\|}}{m^*} \cos\theta \ \tau(\mathbf{k}) \tag{3.12}$$

with the relaxation time being given in equation (3.10).

Now that the distribution function has been established, we can calculate the current density and electron density needed to find the mobility:

$$J_z = -\frac{e}{4\pi^3} \int g_z(\mathbf{k}) v_z(\mathbf{k}) \ d\mathbf{k} \tag{3.13}$$

and

$$n = \frac{1}{4\pi^3} \int f_0(\mathbf{k}) \ d\mathbf{k} \tag{3.14}$$

The θ-integral of equation (3.13) can be performed trivially, which leaves a two-dimensional $(k_{\|}, k_z)$ integral which is calculated numerically in most cases.

The calculations for the acoustic phonon scattering case were all done with the temperature set at 20K. At this temperature the acoustic phonon scattering becomes more important than polar optic scattering due to the larger energy, and hence the lower density, of the optic phonons. We also use an alloy concentration of $x = 0.3$, which means that the alloy bandstructure has a direct bandgap, and a barrier height of $\approx 250meV$.

The first graph, figure 3.2, shows the variation of the mobility parallel to the layers, $\mu_{\|}$, with the superlattice period d, and is similar to the results given by Palmier and Chomette (1982). The statistics are Boltzmann statistics, with the Fermi level well down in the band gap.

If the approximation is made that the relaxation time is constant and equal to the relaxation time at the top of the miniband then, for Boltzmann statistics, the integrals can be performed analytically to give the mobility as,

$$\mu_{\|} = \frac{\hbar^3 e \beta S^2 \rho d}{E_1^2 m^{*2}} \tag{3.15}$$

Examining equations (3.10) and (3.11) it is evident that, as the relaxation time is energy dependent within the miniband and constant above the top of the miniband, the approximation of taking a constant relaxation time will be more accurate for narrow minibands. From figure 3.2 it can be seen that for d larger than ≈ 150Å, where the miniband is indeed narrow, the above equation (3.15) holds true and the mobility is proportional to the period. However, for lower periods, the variation of the relaxation time through the miniband becomes important and equation (3.15) is no longer valid. The relaxation times below the top of the miniband now become the ones that dominate the transport. As the relaxation times at these energies are larger, the mobility shows an increase as the period is further reduced.

Figure 3.3 shows the variation of the mobility parallel to the layers, $\mu_{\parallel}$, with chemical potential for a superlattice with a period of 70Å. The mobility can be seen to fall as the chemical potential is moved up through the miniband. This is due to the increase in the final density of states at the Fermi level as the energy increases, increasing the scattering rate for the electrons at the Fermi energy, which are the ones that contribute to the transport when the Fermi level is well in the band. As the Fermi level is taken above the top of the miniband the mobility becomes constant, reflecting the constant density of states in this region.

Finally, figure 3.4 shows the variation of the mobility in the Boltzmann regime with temperature. It shows the expected decrease in mobility as the temperature is raised due to the increase in the density of phonons. The form of the falloff is close to a 1/T variation as predicted by equation (3.15).

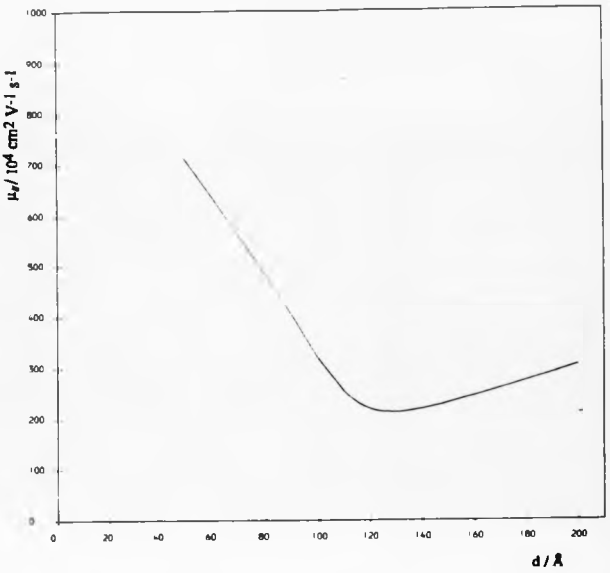

Figure 3.2: The mobility parallel to the superlattice layers as a function of superlattice period. The statistics are Boltzmann and the temperature is 20K. The scattering is by acoustic phonons.

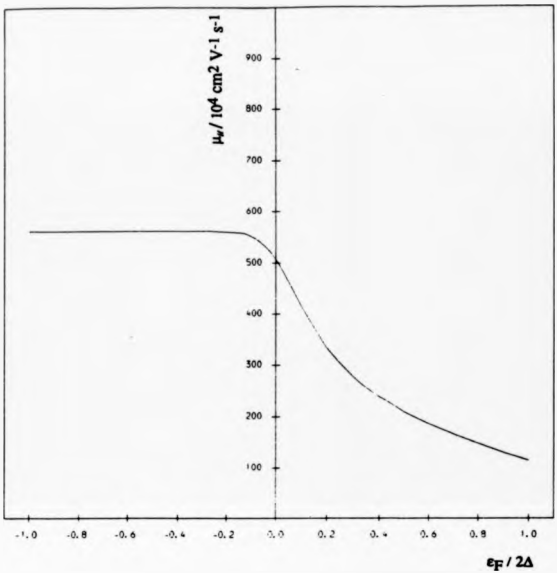

Figure 3.3: The mobility parallel to the superlattice layers as a function of Fermi level. The temperature is 20K and the period is 70Å (well width = barrier width). The scattering is by acoustic phonons.

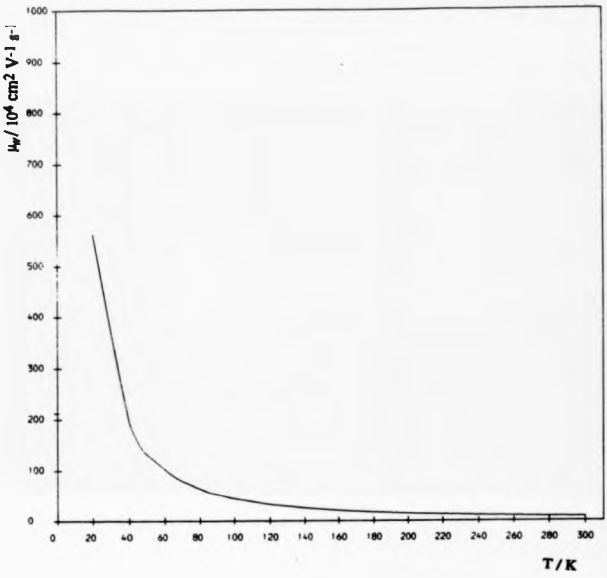

Figure 3.4: The mobility parallel to the superlattice layers as a function of temperature. The statistics are Boltzmann and the period is 70Å (well width = barrier width). The scattering is by acoustic phonons.

3.2.2 . Polar Optic Phonon Scattering

At high temperatures, the dominant scattering mechanism in GaAs, which is a strongly polar material, is polar optic phonon scattering. Transport limited by polar optic phonons is much more difficult to treat than the acoustic phonon limited case due to the highly inelastic nature of the mechanism. This means that a relaxation time cannot be exactly defined for this process.

The calculation has however been carried out under the relaxation time approximation (Palmier and Chomette, 1982) by defining the relaxation time simply as the intrinsic lifetime of an electron in a state $|\mathbf{k}>$.

$$\tau(\mathbf{k}) = \{\int P(\mathbf{k},\mathbf{k}')\ d\mathbf{k}'\}^{-1} \tag{3.16}$$

The method used here is the iterative method described in chapter 2, developed from a method formulated by Rode (1970). The transition rate used here is the Fröhlich scattering rate, equation (2.34)

$$P(\mathbf{k},\mathbf{k}') = \frac{e^2\omega_0}{8\pi^2\epsilon_0}\left(\frac{1}{\kappa_\infty}-\frac{1}{\kappa_0}\right)\frac{(N_0+1/2\pm1/2)}{|\mathbf{k}-\mathbf{k}'|}\delta(\epsilon(\mathbf{k}')-\epsilon(\mathbf{k})\pm\hbar\omega_0) \tag{3.17}$$

with the polar optic phonon frequency being treated as a constant.

Inserting the scattering rate (3.17) into the iterative equation (2.26), the three-dimensional integral can then be reduced to a one-dimensional integral over k_z' (see appendix B),

$$\tilde{g}_{i+1}(\mathbf{k}) = \frac{2\pi\gamma\int_{\Gamma\pm} dk_z'\left\{\frac{\hbar F}{e}\left[\frac{k}{(k^2-c^2)^{1/2}}-1\right]\right\} + \frac{1}{2}E\beta f_0(1-f_0)\frac{k_\parallel^2}{m^*}k_\parallel}{2\pi\gamma\int_{\Gamma\pm} dk_z'\left\{\frac{(1-f_0')|N_0+1/2\pm1/2|+f_0'|N_0+1/2\mp1/2|}{(k^2-c^2)^{1/2}}\right\}} \tag{3.18}$$

and

$$g_{i,z}(\mathbf{k}) = \tilde{g}_i(k_\parallel,k_z)\ \cos\theta \tag{3.19}$$

In equation (3.18), the following variables have been defined.

$$\gamma = \frac{e^3\omega_0}{8\pi^2\epsilon_0}\left(\frac{1}{\kappa_\infty} - \frac{1}{\kappa_0}\right)\frac{m^*}{\hbar^2} \tag{3.20a}$$

$$F(k_\parallel, k_z) = (1 - f_0)[N_0 + 1/2 \mp 1/2] + f_0[N_0 + 1/2 \pm 1/2] \tag{3.20b}$$

$$b = k_\parallel'^2 + k_\parallel^2 + (k_z' - k_z)^2 \tag{3.20c}$$

$$c = 2k_\parallel' k_\parallel \tag{3.20d}$$

with $k_\parallel'$ evaluated as a function of k_z', knowing that the final electron energy is $\epsilon(\mathbf{k}) \pm \hbar\omega_0$, ie.

$$k_\parallel' = \left\{\frac{2m^*}{\hbar^2}[\epsilon_z(k_z) - \epsilon_z(k_z') \mp \hbar\omega_0] + k_\parallel^2\right\}^{1/2} \tag{3.21a}$$

$$= \left\{\frac{2m^*}{\hbar^2}[\Delta(\cos k_z' d - \cos k_z d) \mp \hbar\omega_0] + k_\parallel^2\right\}^{1/2} \tag{3.21b}$$

The limits of the integrals, $\Gamma^\pm$, are given in table 3.1.

Figure 3.5 shows the variation of the parallel mobility, $\mu_\parallel$, as the period is varied. Both the relaxation time approximation and the converged iterative solution are shown. The form of the graph is similar to the acoustic phonon limited case, but the mobility is several orders of magnitude smaller. This is due to the increased number of phonons at the higher temperature, and also the stronger electron-phonon interaction for polar optic phonons.

The full curve gives the converged iterative result, and it is evident that it deviates significantly from the relaxation time approximation result, being up to a factor of two larger. Thus, the inclusion of the 'scattering-in' terms in the BTE is necessary for this calculation, and the relaxation time approximation is inadequate.

It is worthwhile making a few remarks on the convergence of this iterative technique. It has been shown by Rode (Rode, 1975) that equation (2.26) is an

example of a contraction mapping when the scattering is polar optic phonon scattering. Once this has been established, it can be said that the sequence of $g_i(\mathbf{k})$'s converges, and that it converges to a unique solution $g_\infty(\mathbf{k})$ that is independent of the starting point. It can also be said that the method converges exponentially. In the calculation presented here, the mobility typically reaches within 5% of its final converged value after four iterations.

Figure 3.6 shows the variation of the mobility parallel to the layers as the chemical potential is varied. The graph shows a decrease in the mobility as the chemical potential moves up through the miniband, and then an increase as the chemical potential is raised above the top of the miniband. The scattering rate is proportional to $1/|\mathbf{k}-\mathbf{k}'|^2 \times$(D.O.S.), and so, as the chemical potential moves through the miniband where the D.O.S. is rapidly increasing, the scattering rises and the mobility falls. However, as the chemical potential is further increased past the top of the miniband, the D.O.S. becomes constant and the scattering rate solely depends on the average value of $1/|\mathbf{k} - \mathbf{k}'|^2$. At higher energies, the magnitude of the Fermi wavevector is larger and so $< 1/|\mathbf{k} - \mathbf{k}'|^2 >$ will decrease as the chemical potential is increased. This leads to a rise in the mobility. Roughly speaking, we can say that $< 1/|\mathbf{k} - \mathbf{k}'|^2 > \approx 1/k_F^2$, where k_F is the Fermi wavevector, and thus $< 1/|\mathbf{k} - \mathbf{k}'|^2 > \approx \epsilon_F^{-1}$. It follows that the mobility, which is proportional to a typical scattering time, or the reciprocal of a scattering rate, varies as ϵ_F. This can be seen in the results shown in figure 3.6.

Energy Range	Limits	
$\epsilon(\mathbf{k}) < \hbar\omega_0$	$\Gamma^+ = \{0, 0\}$	$\Gamma^- = \{-k^-, k^-\}$
$\hbar\omega_0 \le \epsilon(\mathbf{k}) < 2\Delta - \hbar\omega_0$	$\Gamma^+ = \{-k^+, k^+\}$	$\Gamma^- = \{-k^-, k^-\}$
$2\Delta - \hbar\omega_0 \le \epsilon(\mathbf{k}) < 2\Delta + \hbar\omega_0$	$\Gamma^+ = \{-k^+, k^+\}$	$\Gamma^- = \{-\pi/d, \pi/d\}$
$2\Delta + \hbar\omega_0 \le \epsilon(\mathbf{k})$	$\Gamma^+ = \{-\pi/d, \pi/d\}$	$\Gamma^- = \{-\pi/d, \pi/d\}$

Table 3.1: The Integration Limits for Equation (3.18)

The (+) and (-) signs correspond to phonon emission and absorption respectively and $k^\pm d = \cos^{-1}\left[\cos k_z d - \frac{\hbar^2 k_\perp^2}{2m^*\Delta} \pm \frac{\hbar\omega_0}{\Delta}\right]$.

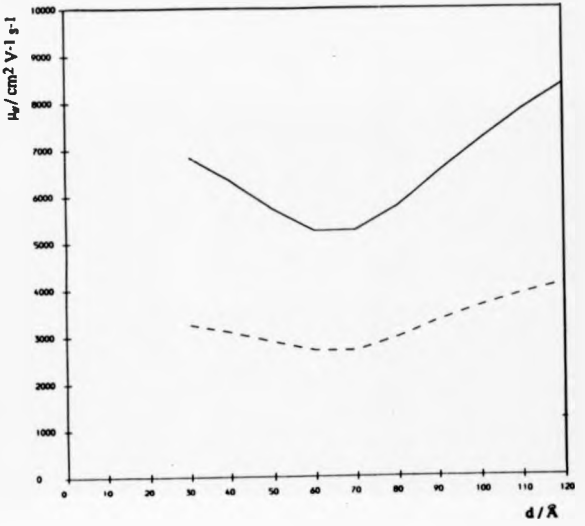

Figure 3.5: The mobility parallel to the superlattice layers as a function of superlattice period. The statistics are Boltzmann and the temperature is 300K. The scattering is by polar optic phonons.

The dashed curve is the relaxation time calculation and the full curve is the iterated solution.

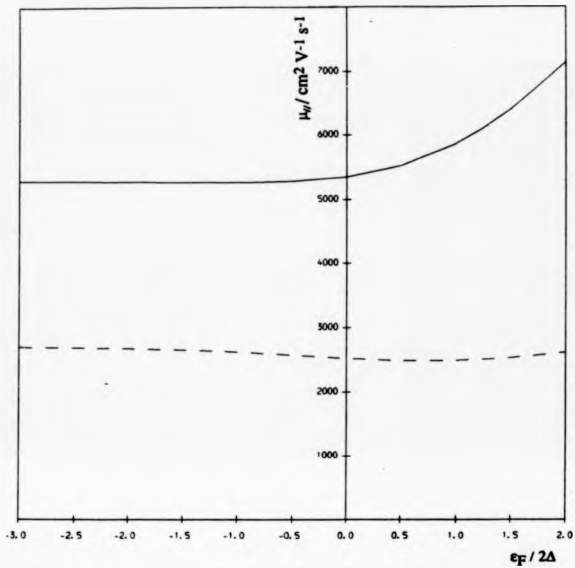

Figure 3.6: The mobility parallel to the superlattice layers as a function of Fermi level. The temperature is 300K and the period is 70Å (well width = barrier width). The scattering is by polar phonons.

The dashed curve is the relaxation time approximation result and the full curve is the iterated solution.

3.3 . Thermopower

The other major electronic transport coefficient studied by experimental and theoretical solid state physicists is thermopower, which is defined in equation (2.15a). The thermopower describes relations between electric and thermal currents. It can be measured by setting up a temperature gradient across a sample and allowing no electric current to flow once a steady state is reached. The induced electric field required to counter the drift of electrons due to the temperature gradient is then measured and the thermopower calculated.

Once the electron distribution has been evaluated for the mobility calculation, the thermopower follows very quickly from some simple numerical integration. It can be simply shown (Blatt, 1968; Butcher, 1973; Ziman, 1972) that the coefficient L of equation (2.13a) is given by

$$L = -\frac{1}{4\pi^3 T}\int \left(\frac{g(\mathbf{k})}{E}\right) \mathbf{v}(\mathbf{k})[\epsilon(\mathbf{k}) - \mu]\ d\mathbf{k} \tag{3.22}$$

and the thermopower is

$$S = -\frac{L}{\sigma} \tag{3.23}$$

An interpretation of thermopower, which follows from the form of equation (3.22), is that it it gives an indication of the average energy above the Fermi energy carried by the electrons contributing to the transport properties. This definition is often useful when attempting to explain physically the thermopower results.

A thermopower calculation has been carried out for a superlattice (Friedman, 1984; Tao & Friedman, 1985) where the electron statistics are taken to be degenerate. In this case, the thermopower is given by the formula (Wilson, 1958)

$$S = -\frac{\pi^2}{3\epsilon} k_B^2 T \left[\frac{\partial}{\partial \epsilon} \ln \sigma(\epsilon)\right]_{\epsilon = \mu} \tag{3.24}$$

where $\sigma(\epsilon)$ is the metallic conductivity with the Fermi energy at the energy ϵ.

The results shown here use the more fundamental definition of thermopower, equations (3.22) and (3.23), and so include effects of thermal broadening and allow for non-degenerate semiconductor statistics.

3.3.1 . Acoustic Phonon Scattering

For Boltzmann statistics, the chemical potential is deep in the band gap, and typical electron energies are thermal energies, of order k_BT. Thus, at low temperatures, we have

$$|\epsilon(\mathbf{k})| \approx k_BT \ll |\mu| \tag{3.25}$$

and the thermopower is immediately given as

$$S \approx \frac{\mu}{eT} \tag{3.26}$$

Figure 3.7 shows the thermopower parallel to the layers as the chemical potential is varied. In the Boltzmann regime, it can be seen that the thermopower does vary linearly with the chemical potential as predicted by equation (3.26). As the chemical potential moves into the miniband, because of the low temperature, the thermopower remains small as only the electrons close to the Fermi level contribute to the transport. It should be noted that the thermopower always remains negative, which is the usual case when the charge carriers are electrons.

Figure 3.8 shows $S_\parallel$ as the superlattice period is varied when the chemical potential is in the centre of the miniband, $\mu = \Delta$. For a period larger than $\approx$ 150Å, where the miniband width becomes of order k_BT, the thermopower becomes independent of d and remains constant at a 2D value. However, When the period is reduced below the '2D value', the thermopower rapidly becomes less negative, even turning positive for very small d. For the smaller values of d, the miniband becomes wider and there are more electron states below the Fermi level. It is the electrons below the Fermi level that give a

positive contribution to the thermopower, and so $S_{\parallel}$ becomes more positive as the period is reduced. Also, the superlattice density of states becomes constant past the top of the miniband, and is less than the '3D D.O.S.' ($\propto \epsilon^{1/2}$) at higher energies. This means that the contribution to the thermopower from the electrons above the Fermi level is reduced, and explains why it is possible for the thermopower to go positive for small superlattice periods.

The final graph for this section, figure 3.9, shows the variation of thermopower $S_{\parallel}$ with temperature, where the chemical potential is in the centre of the miniband. It can be seen that as the temperature becomes low, the electron statistics are becoming degenerate and only electrons close to the Fermi level are contributing to the transport. Thus the thermopower becomes small as the temperature is reduced, approaching zero as the temperature tends towards zero Kelvin.

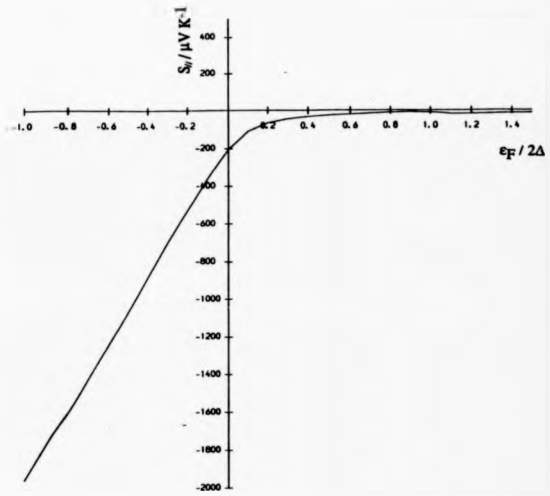

Figure 3.7: The thermopower parallel to the superlattice layers as a function of Fermi level. The temperature is 20K and the period is 70Å (well width = barrier width). The scattering is by acoustic phonons.

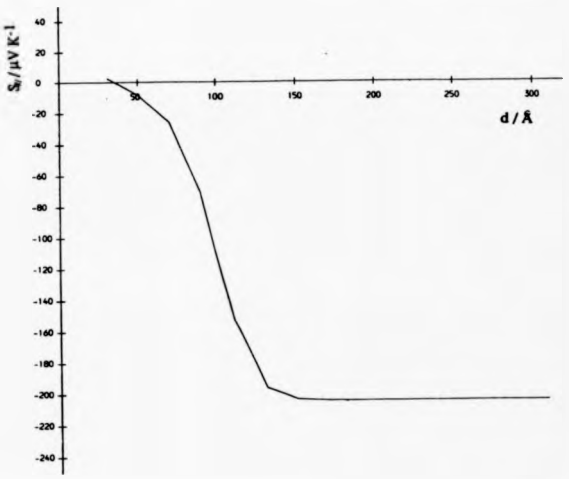

Figure 3.8: The thermopower parallel to the superlattice layers as a function of superlattice period. The temperature is 20K and the Fermi level is at the centre of the miniband ($\varepsilon_F = \Delta$). The scattering is by acoustic phonons.

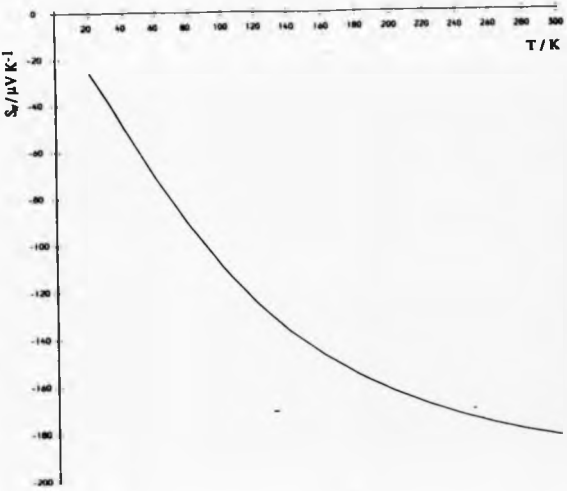

Figure 3.9: The thermopower parallel to the superlattice layers as a function of temperature. The period is 70Å (well width = barrier width) and the Fermi level is at the centre of the miniband ($\varepsilon_F = \Delta$). The scattering is by acoustic phonons.

3.3.2 . Polar Optic Phonon Scattering

We now move on to the polar optic phonon scattering case, where the thermopower is evaluated by the iterative technique.

The first calculation is the variation of thermopower, $S_{\|}$, as the chemical potential is varied from within the band gap and up through the miniband, as shown in figure 3.10. The calculation was carried out for T=300K, where polar optic phonon scattering is dominant.

Due to the large degree of thermal broadening at high temperatures, the curve is much smoother that the acoustic phonon calculation for T=20K, but it is still evident that the thermopower becomes less negative as the chemical potential is increased. The magnitude of the thermopower remains large

as the chemical potential varies, which is typical of a non-degenerate system. Degenerate metals have a typical thermopower of $|S| < 10\mu V/K$ at room temperature compared to $\approx 200\mu V/K$ here.

The next graph for polar optic phonon scattering, figure 3.11, shows $S_{\|}$ against temperature. It shows the same general trend as for the case of acoustic phonon scattering, that is a reduction in $S_{\|}$ as the temperature is lowered. However, at lower temperatures, $S_{\|}$ does remain at a larger magnitude than when acoustic phonons were considered. This could be due to the much reduced strength of the optical phonon scattering at low temperatures, where the density of the high energy optic phonons is small.

This is the final set of results for this chapter for the transport parallel to the layers. In the next chapter we give the results for transport perpendicular to the layer planes. There are similarities between the sets of results, but the differences are highlighted.

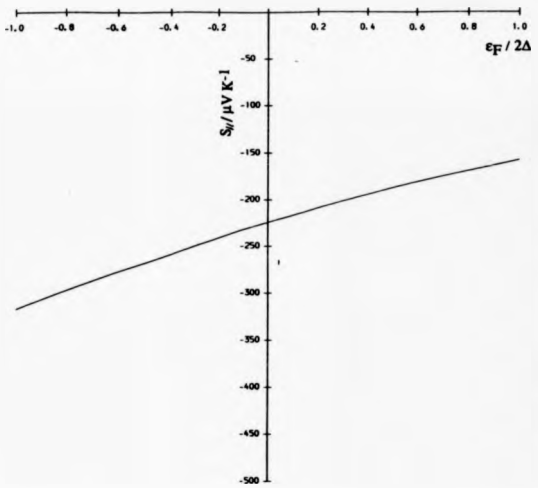

Figure 3.10: The thermopower parallel to the superlattice layers as a function of Fermi level. The temperature is 300K and the period is 70Å (well width = barrier width). The scattering is by polar optic phonons.

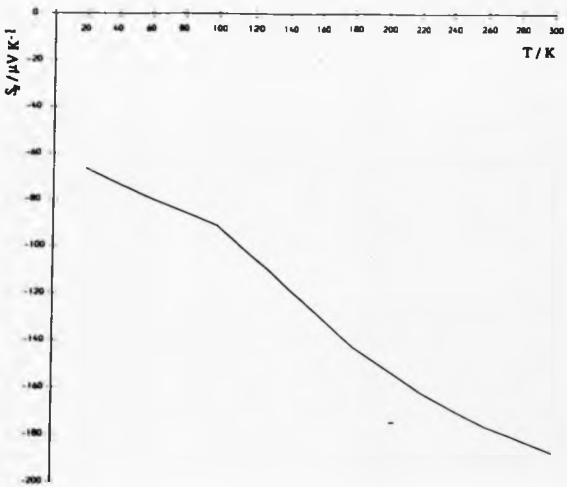

Figure 3.11: The thermopower parallel to the superlattice layers as a function of temperature. The period is 70Å (well width = barrier width) and the Fermi level is at the centre of the miniband ($\varepsilon_F = \Delta$). The scattering is by polar optic phonons.

CHAPTER 4

Vertical Transport

4.1 . Introduction

There are two distinct approaches to treating vertical transport, that is transport in the growth direction of a superlattice. The first is to treat the electron wavefunctions as localised in the growth direction, with the electrons spending most of their time in the GaAs wells. The transport is then treated as a hopping problem, with phonon assisted tunneling of the electrons through the barriers. This method is suitable for superlattices with wide barriers, and has been adequatly treated (Calecki et al, 1984; Palmier et al, 1985).

The second method, which is more suitable for superlattices with narrower layers, is to treat the electron wavefunctions as extended throughout the system, in which case the transport can be described using the semiclassical Boltzmann equation. This is the approach that is followed here.

As yet, a calculation that combines the two approaches, examining the crossover between the localised and extended state transport has not been carried out.

When the idea of a superlattice was first proposed (Esaki and Tsu, 1970), it was the possibility of observing Bloch oscillations, producing negative differential resistance, that was the main source of interest in the system, so it is clear that vertical transport has always been at the forefront of superlattice studies.

4.2 . Mobility

4.2.1 . Acoustic Phonon Limited Mobility

As we have seen in chapter three, the Boltzmann equation can be treated with the relaxation time approximation when deformation potential scattering is considered, and the relaxation time is given by equations (3.10) and (3.11).

$$\frac{1}{\tau_{ac}(\epsilon)} = \frac{E_1^2 m^* k_B T}{\pi S^2 \rho \hbar^3 d} \cos^{-1}\left\{1 - \frac{\epsilon(\mathbf{k})}{\Delta}\right\} \qquad ;\epsilon(\mathbf{k}) < 2\Delta$$

$$= \frac{E_1^2 m^* k_B T}{S^2 \rho \hbar^3 d} \qquad ;\epsilon(\mathbf{k}) \geq 2\Delta \qquad (4.1)$$

The distribution function perturbation with the electric field in the growth direction (z-axis) follows from equations (2.23) and (2.25).

$$g_z(\mathbf{k}) = \frac{e}{\hbar} E_z \frac{\partial f_0}{\partial k_z} \tau_{ac}(\epsilon) \qquad (4.2a)$$

$$= \frac{e}{\hbar} E_z \frac{df_0}{d\epsilon} \Delta d \sin k_z d \ \tau_{ac}(\epsilon) \qquad (4.2b)$$

Figure 4.1 shows the variation of the mobility in the growth direction, μ_z, with the superlattice period for Boltzmann statistics.

As the period is increased, the mobility can be seen to fall very rapidly. As the width of the barriers becomes larger, the electron states become more localised within the wells and the probability of tunneling through the barriers becomes exponentially less. This gives rise to the exponential fall in the mobility as the period is increased.

The next graph, figure 4.2, shows μ_z as the chemical potential is varied. The mobility is independent of the chemical potential in the Boltzmann regime and then falls as the chemical potential moves through the miniband. This is similar to the behaviour of $\mu_{\parallel}$, the decrease in both cases being due to the

increase in the density of states, and hence the scattering rates, higher up in the miniband. However, μ_z becomes much smaller for larger values of d, and does not show such a clear levelling off past the top of the miniband. So, when the chemical potential is above the top of the miniband, in the '2D regime', the vertical transport parameter, μ_z, is limited more than the parallel mobility, $\mu_{\parallel}$.

Finally, figure 4.3 shows μ_z versus temperature, and shows the same features as the parallel transport equivalent, figure 3.4.

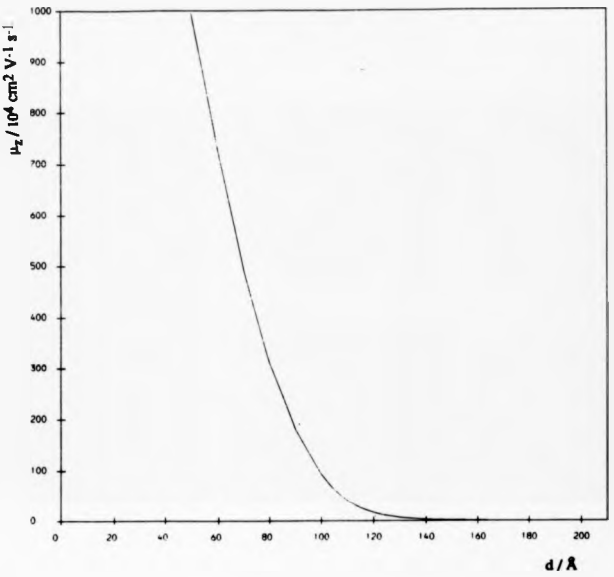

Figure 4.1: The mobility in the superlattice growth direction as a function of superlattice period. The statistics are Boltzmann and the temperature is 20K. The scattering is by acoustic phonons.

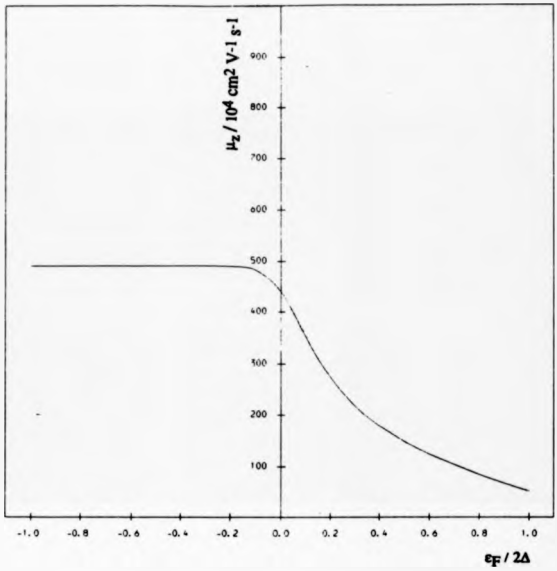

Figure 4.2: The mobility in the superlattice growth direction as a function of Fermi level. The temperature is 20K and the period is 70Å (well width = barrier width). The scattering is by acoustic phonons.

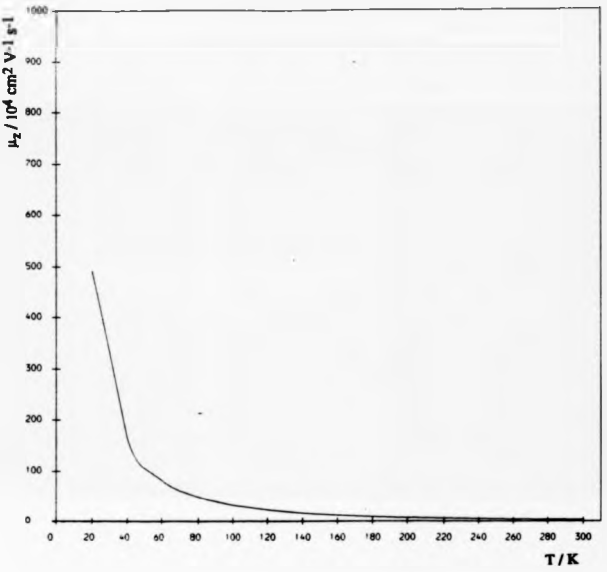

Figure 4.3: The mobility in the superlattice growth direction as a function of temperature. The statistics are Boltzmann and the period is 70Å (well width = barrier width). The scattering is by acoustic phonons.

4.2.2 . Polar Optic Phonon Limited Mobility

For transport in the growth direction, the derivation of the iterative equation for the perturbation to the Boltzmann distribution function, $g(\mathbf{k})$, follows in the same manner as for the parallel transport case. There is however one simplification in this case. Due to the cylindrical symmetry of the superlattice, we can say immediatly that, when the electric field is along the growth direction, there is no θ-dependence in the distribution function. Inserting the polar optic phonon scattering rate, equation (3.17), into the iterative equation (2.26), with the electric field along the z-axis, then produces,

$$\left[\frac{g(k_\parallel,k_z)}{E}\right]_{i+1} = \frac{2\pi\gamma \int_{\Gamma\pm}\{[g(k'_\parallel,k'_z)/E]_i I\}\ dk'_z + \frac{q}{\hbar}\beta f_0(1-f_0)\frac{\partial L}{\partial k_z}}{2\pi\gamma \int_{\Gamma\mp} I'\ dk'_z} \tag{4.3}$$

where

$$I \equiv \frac{(1-f_0(\mathbf{k}))|N+1/2\mp 1/2| + f_0(\mathbf{k})|N+1/2\pm 1/2|}{[(k_\parallel^2-k_\parallel'^2)^2+2(k_\parallel^2+k_\parallel'^2)(k_z-k'_{\parallel})^2+(k_z-k'_z)^4]^{1/2}} \tag{4.4}$$

and I' has a similar definition, but with $f_0(\mathbf{k}')$ replacing $f_0(\mathbf{k})$ in the numerator. The limits of integration are given in table 3.1, and $k'_\parallel$ is expressed as a function of k'_z in equation (3.21).

If the calculation is for the Boltzmann regime, the integrals can be simplified, with I and I' being replaced by,

$$I_{BOL} = \frac{(N+1/2\mp 1/2)}{[(k_\parallel^2-k_\parallel'^2)^2+2(k_\parallel^2+k_\parallel'^2)(k_z-k'_z)^2+(k_z-k'_z)^4]^{1/2}} \tag{4.5}$$

As before, equation (4.3) can be solved by iterating numerically, starting with the initial solution of $g(\mathbf{k})=0$.

The iterated solution to equation (4.3) is shown as a two dimensional plot in figure 4.4. The picture shows several marked features. First, there is a kink in the surface at an energy of $2\Delta-\hbar\omega_0$. At this energy, electrons being scattered by phonon absorption are scattered to the top of the miniband, where there is a sharp change in the form of the density of states, causing the observed kink

in the distribution function.

Next, there is a rapid fall in the distribution function at an energy of $\hbar\omega_0$. This is due to the onset of the phonon emission process. Finally, kinks are seen in the distribution function at energies of $2\hbar\omega_0$, $3\hbar\omega_0$. When an electron with energy $2\hbar\omega_0$ is scattered by phonon emission, its final state has energy $\hbar\omega_0$. As we have seen, the distribution function at an energy of $\hbar\omega_0$ has a kink, and so there is a gradient discontinuity in the density of final states available to an electron being scattered from an energy of $2\hbar\omega_0$. This gives rise to the kink in the distribution function at $2\hbar\omega_0$, with a similar explanation for the feature at $3\hbar\omega_0$.

It should be noted that the above explanation is of physical origin, and is not just due to the nature of the iterative equation. However, it is the iterations that produce the features, and they are totally absent when the calculation is solved using the relaxation time approximation, which is equivalent to one iteration of equation (4.3).

Once the distribution function has been obtained, the mobility follows as before, using equations (3.13) and (3.14).

Figure 4.5 shows the variation of the vertical mobility, μ_z, as the superlattice period d is varied. The calculation was for a temperature of 300K, with the Fermi level at the bottom of the miniband. The graph shows both the solution evaluated under the relaxation time approximation and the iterative solution. The iterative solution is up to a factor of two larger than the relaxation time result, which again shows the importance of the 'scattering-in' terms of the Boltzmann equation when polar optic scattering is considered in the superlattice system. The mobility shows the same rapid fall for larger periods as for the acoustic case, and for small periods the mobility approaches a typical bulk value for the materials being examined. This is because, for narrower layers, the superlattice band structure becomes less anisotropic and more like a bulk band structure.

Finally, in this section, figure 4.6 shows μ_x versus Fermi level. It shows a similar form to μ_x in the acoustic limited case, but is smoother due to the higher temperature and the inelastic nature of the scattering mechanism.

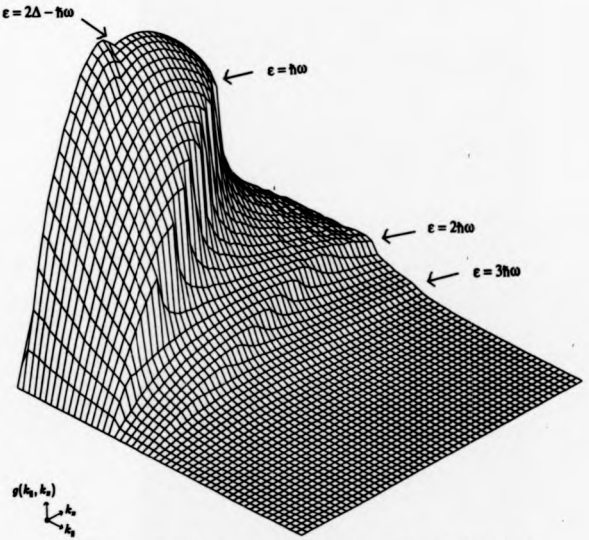

Figure 4.4: A surface plot of the distribution function $g(k_y,k_z)$ when the applied electric field is in the superlattice growth direction.

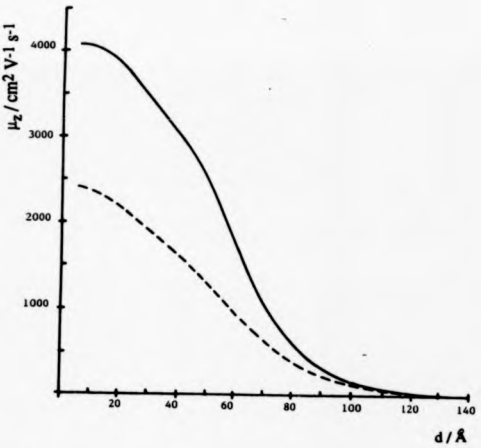

Figure 4.5: The mobility in the superlattice growth direction as a function of superlattice period. The statistics are Boltzmann and the temperature is 300K. The scattering is by polar optic phonons.

The dashed curve is the relaxation time calculation and the full curve is the iterated solution.

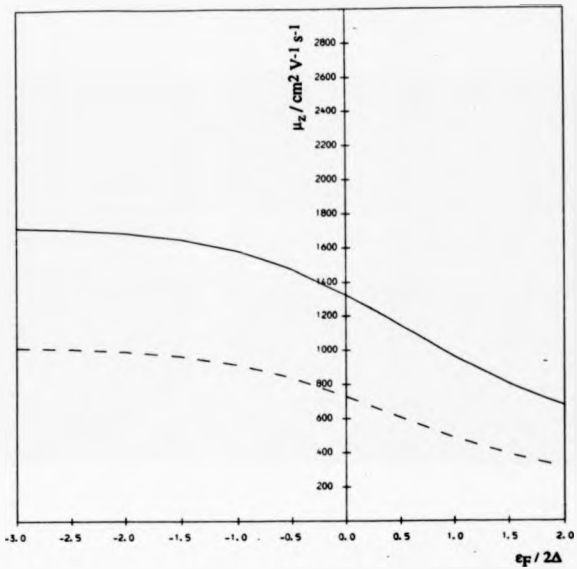

Figure 4.6: The mobility in the superlattice growth direction as a function of Fermi level. The temperature is 300K and the period is 70Å (well width = barrier width). The scattering is by polar optic phonons.

The dashed curve is the relaxation time approximation result and the full curve is the iterated solution.

4.3 . Thermopower

In this section we give the thermopower results for a superlattice when the temperature gradient and resulting opposing electric field are along the growth direction. These results are then compared with the corresponding results in section 3.4 for parallel transport.

4.3.1 . Acoustic Phonon Scattering

The calculation of the vertical thermopower, S_z, limited by acoustic phonon scattering at a temperature of 20K is shown in figure 4.7 as a function of Fermi level. The general features are similar to the parallel transport case shown in figure 3.7 and discussed in section 3.4.1. The curve has a linear variation with μ in the Boltzmann regime and then S_z has a small value when the electron statistics are degenerate and the Fermi level is within the miniband.

The clear difference between the two curves is when the Fermi level is close to the top of the miniband. In this case, the thermopower exhibits a positive peak as the Fermi level moves past the top of the miniband. Similar features have been noted in calculations for quasi-1D systems (Kearney and Butcher, 1986) and 2D systems (Cantrell and Butcher, 1985). These systems also show a rapid variation in the density of states at the energies where positive thermopower peaks are observed. It is this singularity in the derivative of the density of states that produces a positive contribution to the thermopower.

However, we do not see the divergence of the thermopower in the calculation of Friedman (1984) using the formula for a degenerate electron gas (Wilson, 1958).

$$S = -\frac{\pi^2}{3e} k_B^2 T \left[\frac{\partial}{\partial \epsilon} \ln \sigma(\epsilon) \right]_{\epsilon=\epsilon_F} \tag{4.6}$$

Friedman points out that the curves he shows do not include thermal broadening, which would reduce the singularity at the top of the miniband to a finite positive peak.

The next graph, figure 4.8, shows the variation of S_z with superlattice period when the Fermi level is in the centre of the miniband. It can be seen that the form is similar to the parallel case, except for the value of the thermopower in the '2D-regime.' The value for the vertical thermopower is lower than for parallel transport by a factor of about two. If the assumption is made that the system is quasi-2D with a constant relaxation time, which is reasonable because the miniband width is very small, $2\Delta \ll k_B T$, then the expressions for the thermopower, equations (3.22) and (3.23) can be reduced to the simple forms,

$$S_z = -\frac{k_B}{e}\frac{\int_0^\infty \frac{x^{1/2}}{(e^x+1)(e^{-x}+1)}\,dx}{\int_0^\infty \frac{x^{-1/2}}{(e^x+1)(e^{-x}+1)}\,dx} \tag{4.7}$$

$$S_\parallel = -\frac{k_B}{e}\frac{\int_0^\infty \frac{x^{3/2}}{(e^x+1)(e^{-x}+1)}\,dx}{\int_0^\infty \frac{x^{1/2}}{(e^x+1)(e^{-x}+1)}\,dx} \tag{4.8}$$

which gives the ratio of S_z and $S_\parallel$ in the 2D regime as,

$$\frac{S_\perp}{S_\parallel} = \frac{\int_0^\infty x^{3/2}\mathrm{sech}^2 x/2\,dx \;\; \int_0^\infty x^{-1/2}\mathrm{sech}^2 x/2\,dx}{\left\{\int_0^\infty x^{1/2}\mathrm{sech}^2 x/2\,dx\right\}^2} \tag{4.9a}$$

$$= \frac{(1-2\sqrt{2})}{(2-\sqrt{2})}\;\frac{\Gamma(5/2)\varsigma(3/2)\Gamma(1/2)\varsigma(-1/2)}{[\Gamma(3/2)\varsigma(1/2)]^2} \tag{4.9b}$$

The integrals in equation (4.9a) are standard (Gradshteyn and Ryzhik, 1980), and the functions $\Gamma(z)$ and $\varsigma(z)$ in equation (4.9b) are the gamma function and the Reimann zeta function respectively. Inserting the values of these functions into the expressions (Jahnke and Emde,1945) gives a value of the ratio of ~ 2.57. This shows that $S_\parallel$ should be larger than S_z, and the reason for the different forms of equations (4.7) and (4.8) is just that the dispersion in the layers is parabolic, and through the layers it is constant.

Finally, similar comments can be made about figure 4.9, the variation of S_z with temperature. It shows a temperature dependence of the same form as $S_\parallel$, with S_z being smaller than $S_\parallel$ by a factor of about two at high temperatures,

where $k_B T$ is becoming comparable with the miniband width.

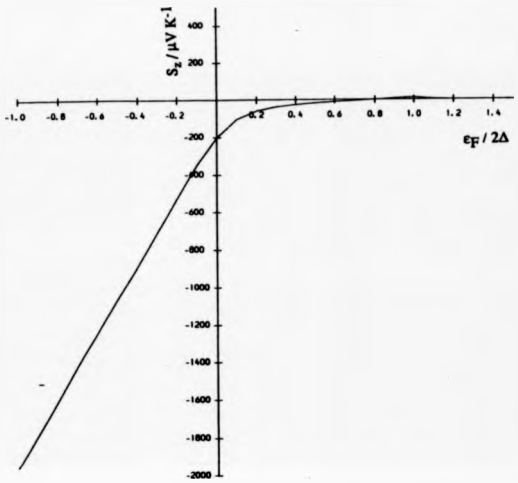

Figure 4.7: The thermopower in the superlattice growth direction as a function of Fermi level. The temperature is 20K and the period is 70Å (well width = barrier width). The scattering is by acoustic phonons.

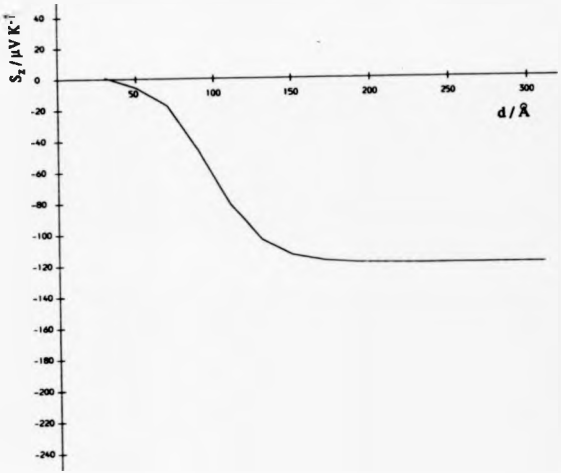

Figure 4.8: The thermopower in the superlattice growth direction as a function of superlattice period. The temperature is 20K and the Fermi level is at the centre of the miniband ($\varepsilon_F = \Delta$). The scattering is by acoustic phonons.

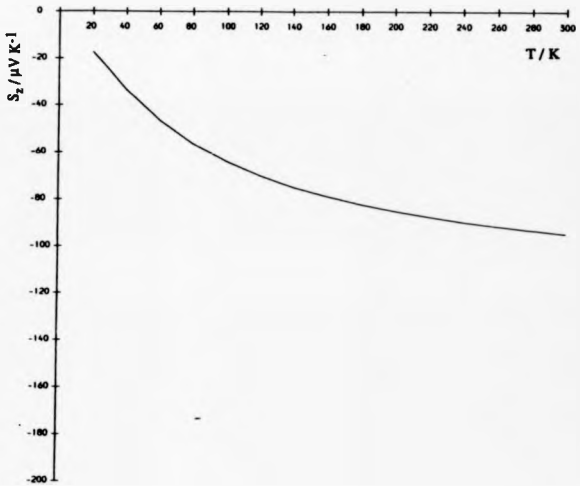

Figure 4.9: The thermopower in the superlattice growth direction as a function of temperature. The period is 70Å (well width = barrier width) and the Fermi level is at the centre of the miniband ($\varepsilon_F = \Delta$). The scattering is by acoustic phonons.

4.3.2 . Polar Optic Phonon Scattering

In the last section of this chapter the results for thermopower limited by optic phonons are presented. The dependence of S_z on Fermi level is shown in figure 4.10. The thermopower shows the gradual rise with increasing Fermi level that was seen for $S_{\|}$, with any sharp features being smoothed out by thermal broadening at the high temperature. However, it can be seen again under the different conditions from the previous section that S_z is smaller in magnitude compared with $S_{\|}$ by a factor of about two, emphasising that it is mainly the form of the superlattice miniband structure that produces this effect.

The final result in this chapter is the temperature dependence of S_z, figure 4.11. The thermopower in this case becomes less negative as the temperature is reduced from 300K, and then becomes more negative as the temperature becomes low. This is similar to $S_{\|}$, but the change in the behaviour at low temperatures is more pronounced here. Again, as we might expect, we see structure in the transport properties being shown more clearly in the vertical transport case than for parallel transport.

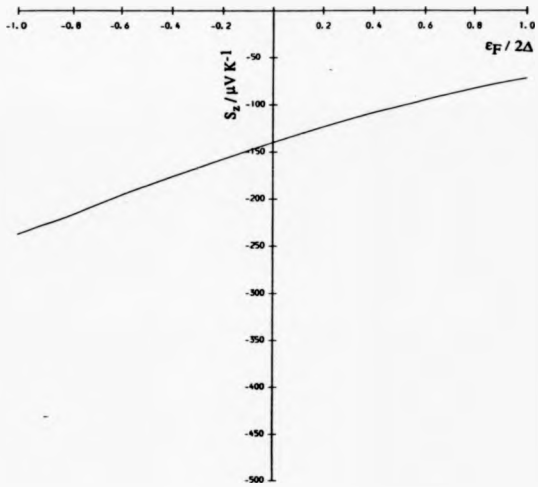

Figure 4.10: The thermopower in the superlattice growth direction as a function of Fermi level. The temperature is 300K and the period is 70Å (well width = barrier width). The scattering is by polar optic phonons.

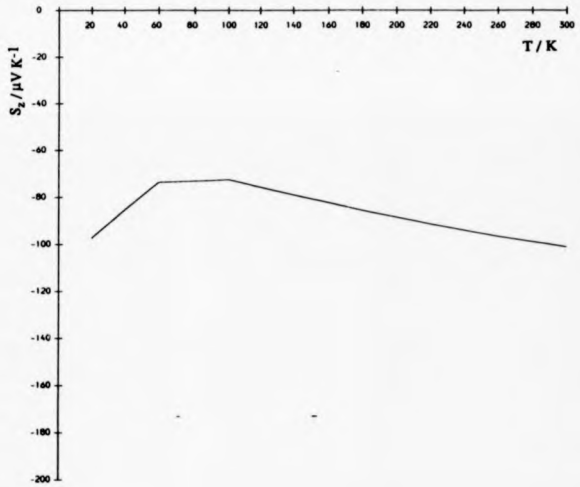

Figure 4.11: The thermopower in the superlattice growth direction as a function of temperature. The period is 70Å (well width = barrier width) and the Fermi level is at the centre of the miniband ($\varepsilon_F = \Delta$). The scattering is by polar optic phonons.

CHAPTER 5

Calculation of the Hall Factors

5.1 . Introduction

In this chapter the effect of a small magnetic field on a superlattice system is analysed. The formalism used to calculate the magnetic field effects is the semi-classical description of the previous chapters, and the full Boltzmann equation with magnetic field included is, in the steady state

$$\mathbf{v}\cdot\nabla f-\frac{e}{\hbar}[\mathbf{E}+\mathbf{v}\times\mathbf{B}]\cdot\nabla_k f=\left(\frac{\partial f}{\partial t}\right)_{COLL} \tag{5.1}$$

which is linearized to give

$$-\frac{e}{\hbar}\mathbf{E}\cdot\nabla_k f_0-(\mathbf{v}\times\mathbf{B})\cdot\nabla_k g=\left(\frac{\partial g}{\partial t}\right)_{COLL} \tag{5.2}$$

It should be noted that the term containing the magnetic field includes the distribution function to first order only. It can be shown simply that the zeroth order contribution is zero (Butcher, 1973).

$$\begin{aligned}-\frac{e}{\hbar}(\mathbf{v}\times\mathbf{B})\cdot\nabla_k f_0 &= -\frac{e}{\hbar}(\mathbf{v}\times\mathbf{B})\cdot\nabla_k\epsilon(\mathbf{k})\frac{df_0}{d\epsilon}\\ &= -e(\mathbf{v}\times\mathbf{B})\cdot\mathbf{v}\frac{df_0}{d\epsilon}\\ &=0\end{aligned} \tag{5.3}$$

With a magnetic field applied, there are many transport parameters that can be studied, such as the Seitz magnetoresistance coefficients, which relate the electric field and current density up to second order in the applied magnetic

field (Butcher, 1973).

$$\mathbf{E}' = \rho_0 \cdot \mathbf{J} - R_0 \mathbf{J} \times \mathbf{B} + \rho_0 \{ b\mathbf{B}^2 \mathbf{J} + c\mathbf{B}(\mathbf{B} \cdot \mathbf{J}) + d\mathbf{D} \cdot \mathbf{J} \} \qquad (5.4)$$

where b, c and d are the Seitz magnetoresistance coefficients and $\mathbf{D}$ is a diagonal tensor, $D_{ii} = B_i^2$. ρ_0 is the resistivity and R_0 is the Hall constant. It is the latter coefficient, R_0, that is examined in this chapter.

While still keeping the applied electric field small, there are several distinct regimes for different magnetic field strengths in the magnetoresistance properties of a system. Firstly, there is the low field limit, which is defined by the relationship $\omega_B \tau << 1$, where $\omega_B = \frac{eB}{m^*}$ is the cyclotron frequency and τ is a typical scattering time. The physical interpretation of this relationship is that the electrons only travel a small distance around a constant energy surface before being scattered. In this case the details of the scattering is usually the most important factor influencing the transport properties. This is the case considered here.

The second regime is the classical high field limit, which has $\omega_B \tau >> 1$, but the magnetic field is not so high that quantum effects are seen in the bandstructure. In this situation, the electrons are able to orbit a constant energy surface many times before being scattered. Thus, the form of the Fermi surface, for example, whether the orbits are open or closed, may have the major influence on the transport properties (Smith, Janak and Adler, 1967). Experiments have been carried out to test for open or closed orbits in superlattices (Sakaki, 1985).

The final case is the quantum high field limit, where Landau levels are formed in the band structure of the system, fundamentally altering the way the electrons behave. This limit is particularly interesting in low dimensional systems, quantum wells and superlattices, as it leads to the phenomenon known as the quantum Hall effect, which has been observed in quasi-2D systems (von Klitzing et al, 1980; von Klitzing 1986). This effect is a direct result of the

modification of the D.O.S. by the high magnetic fields.

To treat the $\mathbf{B}\cdot\nabla_{\vec{R}}$ with a magnetic field included, it if often written in terms of operators. The linearized Boltzmann equation can be expressed in the form

$$(C + \Omega')\phi(\mathbf{k},\mathbf{r}) = -\mathbf{X}\cdot\mathbf{v}\frac{df_0}{d\epsilon} \tag{5.5}$$

In this equation, the distribution function $\mathbf{g(k,r)}$ is transformed into the function $\phi(\mathbf{k},\mathbf{r})$ as follows.

$$g(\mathbf{k},\mathbf{r}) = -\phi(\mathbf{k},\mathbf{r})\frac{df_0}{d\epsilon} \tag{5.6}$$

Now, $\phi(\mathbf{k},\mathbf{r})$ is to be determined from equation (5.5).

On the L.H.S. of equation (5.5) the scattering is given by the collision operator, defined as

$$C\phi(\mathbf{k},\mathbf{r}) = \left(\frac{\partial g}{\partial t}\right)_{COLL} \tag{5.7}$$

and the magnetic effects included through the magnetic operator,

$$\Omega'\phi(\mathbf{k},\mathbf{r}) = -\frac{df_0}{d\epsilon}\frac{e}{\hbar}(\mathbf{v}\times\mathbf{B})\cdot\nabla_k\phi(\mathbf{k},\mathbf{r}) \tag{5.8}$$

The R.H.S. of equation (5.5) gives the driving term, with $\mathbf{X}$ defined as

$$\mathbf{X} = e\mathbf{E}' + \nabla T\frac{\epsilon(\mathbf{k})-\mu}{T} \tag{5.9}$$

The inclusion of the electromotive force, $\mathbf{E}' = \mathbf{E} + \frac{1}{e}\nabla\mu$, and the temperature term on the R.H.S. of equation (5.9) includes the effects of spatial variation in chemical potential and temperature.

One immediate advantage of treating the BTE in this way is that from the symmetry of the formal solution to equation (5.5),

$$\phi = -(C+\Omega')^{-1}\mathbf{X}\cdot\mathbf{v}\frac{df_0}{d\epsilon} \tag{5.10}$$

the Onsager relations (Madelung, 1978; Onsager, 1931); can be derived. The relation that is used later in this chapter to simplify the conductivity tensor is,

$$\sigma_{ij}(\mathbf{B}) = \sigma_{ji}(-\mathbf{B}) \tag{5.11}$$

The most common approach to obtain the transport parameters with a magnetic field present is to proceed within the relaxation time approximation via the Jones-Zener expansion (Jones and Zener, 1934). From the definition of the relaxation time, equation (2.25), the collision term in equation (5.7) is

$$C = \frac{df_0}{d\epsilon}\,\tau^{-1} \tag{5.12}$$

Now if the relaxation time is a function of energy only, which is not always true for a superlattice with a highly anisotropic band structure, then it is evident that the collision operator and the magnetic operator commute, in which case the formal solution to the linearized BTE can be expanded to give, from equations (5.10) and (5.12)

$$\phi = -[1 - \tau\Omega + (\tau\Omega)^2 + \ldots]\,\tau\mathbf{X}\cdot\mathbf{v} \tag{5.13}$$

where $\Omega = \Omega / \frac{d\epsilon}{dk}$

The magnitude of $(\tau\Omega)$ increases linearly with magnetic field, and there will be some critical magnetic field at which the series in equation (5.13) will not converge. This introduces another low magnetic field limit along with $\omega_B\tau < 1$, and it is usually assumed that the magnetic field is below this critical value.

The problem now is as before, finding the form of the relaxation time. When the relaxation time has been found, successive terms of equation (5.13) can be inserted into the integrals for the transport properties, equations (3.13), (3.14) and (3.22), to give the coefficients to increasing order in magnetic field. There are many analyses that produce expressions for the magneto-transport coefficients in certain limits using the Jones-Zener expansion (Butcher, 1973;

Smith, Janak and Adler, 1967).

If the relaxation time approximation, and hence the Jones-Zener expansion cannot be used, then there are few methods that can be used. The variational method can be used to solve the $\mathbf{B} \neq 0$ BTE (Garcíer – Moliner and Simons, 1957) without invoking the relaxation time approximation, but with the highly anisotropic bandstructure of a superlattice system, the analysis would be difficult.

Another method is one proposed by P.J.Price (Price, 1957, 1958). This involves finding a vector l, the 'mean free path for electric currents,' which contains information of the effect of the bandstructure and scattering on the electrons, but does not include any magnetic field effects. Once this vector has been found, it is a simple matter to evaluate the Hall constant by means of a differential operator defined by Price. However, to practically solve the equations for l, Price either follows a relaxation time approximation approach where valid, or otherwise a variational method. Thus the problems encountered before also occur using Price's method.

A method that is practically used to obtain results is the monte carlo method (Jacobini and Reggiani, 1983). This is a numerical simulation of the electron system under the application of electric and magnetic fields, with the macroscopic observables being obtained at the end of the simulation with an averaging process, either time-averaging the variables of a single electron for a homogeneous, steady state problem or otherwise an ensemble average of many simulations. However, the inclusion of a magnetic field reduces the symmetry of the problem, and the drift velocity is no longer parallel to the electric field even for spherical bands. Usually in this case, a full three dimensional simulation is needed, which increases the computing time required significantly. Nevertheless, this approach is still a practical method.

In this chapter is presented a method to calculate the Hall factor to first order in the applied magnetic field that does not rely on the relaxation time approximation or the Jones-Zener expansion. Neither does it depend on the

zero magnetic field distribution function being calculated in a specific way. If the distribution function is known for three mutually perpendicular directions of the applied electric field for a general anisotropic system, then the Hall factors can be calculated simply.

Before this method is presented, the symmetry of the system is examined to decide how best to present the Hall effect results in an anisotropic system where the transport coefficients are tensors.

Finally, Hall factor results are presented using the results calculated in chapters three and four. No further large calculations are needed to evaluate the Hall factors.

5.2 . Symmetry Considerations

When dealing with the magnetic transport properties of a superlattice, the tensor nature of the transport coefficients must be considered due to the highly anisotropic nature of the system. In this section it is shown how the superlattice symmetry affects the components of the transport tensors. The general equation for the ohmic current density to first order in the magnetic field is,

$$J_\alpha = \sum_\beta \sigma_{\alpha\beta} E_\beta + \sum_{\beta,\gamma} C_{\alpha\beta\gamma} E_\beta B_\gamma \tag{5.14}$$

Here, $\sigma_{\alpha\beta}$ is a rank two conductivity tensor that gives the current density to zeroth order in the magnetic field $\mathbf{B}$ and $C_{\alpha\beta\gamma}$ is a rank three tensor that gives the first order terms.

In the simple effective mass representation given here, the cylindrical symmetry of the superlattice system is described by the crystal point group 4/mmm. The Onsager relations (Smith, Janak and Adler, 1967) are used in conjunction with the point group symmetry to reduce $\sigma_{\alpha\beta}$ and $C_{\alpha\beta\gamma}$ to the fewest number of independent parameters possible. Some simple group theoretical arguements (appendix A) can be used to show that both σ and C can be expressed by two parameters each (Smith, Janak and Adler, 1967).

$$\sigma_{xx} = \sigma_{yy} = \sigma_\parallel \tag{5.15a}$$

$$\sigma_{zz} = \sigma_z \tag{5.15b}$$

with all other components zero, and

$$C_{xyz} = -C_{yzx} = \eta \tag{5.16a}$$

$$C_{yzz} = C_{zxy} = -C_{zyz} = -C_{zzy} = \varsigma \tag{5.16b}$$

with all other components zero.

Using the form of the tensors described by equations (5.15) and (5.16), the ohmic current can be written in a simplified form,

$$\mathbf{J} = \sigma\mathbf{E} + \varsigma\mathbf{E} \times \mathbf{B}_{\parallel} + \eta\mathbf{E} \times \mathbf{B}_z \tag{5.17}$$

where $\mathbf{B}_{\parallel} = (B_x, B_y, 0)$ and $\mathbf{B}_z = (0, 0, B_z)$.

It is usually of more use if equation (5.17) is inverted so that the electric field is expressed in terms the current density and the magnetic field. To first order in $\mathbf{B}$, this expression is,

$$\mathbf{E} = \sigma^{-1}\mathbf{J} - \varsigma\sigma^{-2}\mathbf{J} \times \mathbf{B}_{\parallel} - \eta\sigma^{-2}\mathbf{J} \times \mathbf{B}_z \tag{5.18}$$

It is now a simple matter to express the Hall constants in terms of the transport parameters by examining equation (5.18). In this case, three Hall constants are needed to describe the system corresponding to the three orientations of mutually orthogonal $\mathbf{J}$, $\mathbf{B}$ and $\mathbf{E}$ vectors. These Hall constants are,

$$\frac{E_x}{J_y B_z} = R_0^{xyz} = -\eta\sigma_{\parallel}^{-2} \tag{5.19a}$$

$$\frac{E_x}{J_z B_y} = R_0^{xzy} = -\varsigma\sigma_x^{-2} \tag{5.19b}$$

$$\frac{E_y}{J_z B_z} = R_0^{yzz} = -\varsigma\sigma_{\parallel}^{-2} \tag{5.19c}$$

where the first superscript gives the direction of the Hall field $\mathbf{E}^H$, the second gives the direction of the current density $\mathbf{J}$ and the third gives the direction of the magnetic field $\mathbf{B}$. These Hall constants are now simply related to the Hall factors.

$$r_{E^H JB} = -ne R_0^{E^H JB} \tag{5.20}$$

In this chapter the results are presented as the Hall factors corresponding to

the three different Hall constants given in equation (5.19). These are preferred to the elements of the magneto-transport tensor C because the Hall effect is well known and thus easier to describe physically. Also, for bulk semiconductors the Hall factors are generally close to 1 (Blatt, 1968) (classical argument gives r=1), and thus the effects of the superlattice quantum confinement can be readily seen by observing how r deviates from 1.

5.3 . Method of Calculation

In the first section of this chapter, the more formal representation of the Boltzmann equation was introduced, where it was shown that the solution to the Boltzmann equation could be written down in the form,

$$\phi = -(C + \Omega')^{-1}\mathbf{X} \cdot \mathbf{v}\frac{df_0}{d\epsilon} \tag{5.21}$$

where the operators C, Ω', the vector $\mathbf{X}$ and the function ϕ are all defined in section 5.1.

Now, if we start with the case with no magnetic field present, we can write down the solution in terms of the inverse collision operator $G_0 \equiv C^{-1}$.

$$\phi = -G_0 e\mathbf{E} \cdot \mathbf{v}\frac{df_0}{d\epsilon} \tag{5.22}$$

In this equation, we have explicitly put in $\mathbf{X} = e\mathbf{E}$. It is worth noting here that the solution in an electric field $\mathbf{E}'$ is similarly given by

$$\phi' = -G_0 e\mathbf{E}' \cdot \mathbf{v}\frac{df_0}{d\epsilon} \tag{5.23}$$

This solution ϕ' will be used later for a system with an electric field $\mathbf{E}$, but with a magnetic field also present.

The solutions written down here, ϕ and ϕ', as we shall presently, are needed to find the Hall current when a magnetic field is present. The solutions ϕ and ϕ' can be found by whatever means we have at our disposal. For the purpose of finding the Hall factors in a superlattice, these solutions have already been calculated in the previous chapters of this thesis using an iterative method, and can be immediately used for the following magnetic field calculations.

Now, for the case where a magnetic field is present, the solution is given

by equation (5.21), which is written as,

$$\phi = -Ge\mathbf{E}\cdot\mathbf{v}\frac{df_0}{d\epsilon} \tag{5.24}$$

where we have introduced the operator $G \equiv (C+\Omega')^{-1}$. That is,

$$(C+\Omega')G = 1 \tag{5.25}$$

Now, we premultiply both sides of equation (5.25) with the previously defined operator G_0, and perform a small amount of manipulation to give

$$G_0(C+\Omega')G = G_0 \tag{5.26a}$$

ie.

$$(1+G_0\Omega')G = G_0 \tag{5.26b}$$

which leads to

$$G = (1+G_0\Omega')^{-1}G_0 \tag{5.27a}$$

$$\simeq (1-G_0\Omega')G_0 \tag{5.27b}$$

to first order in $\mathbf{B}$. For the very simple case of spherical energy bands and a definable relaxation time that is dependent on energy alone, the condition for the magnetic field to be small is the same as the condition encountered in section 5.1, $\omega_B\tau << 1$.

Now, the solution ϕ can be found from equations (5.24) and (5.27). The term in ϕ that is of interest here is the one that is linear in the magnetic field $\mathbf{B}$ and which determines the resultant Hall current.

$$\Delta\phi = G_0\Omega' G_0\ e\mathbf{E}\cdot\mathbf{v}\frac{df_0}{d\epsilon} \tag{5.28}$$

If $\Delta\phi$ is inserted into the expression for the current density, equation (3.13), then we obtain the Hall current.

$$\mathbf{J}_H = -\frac{e}{4\pi^3}\int d\mathbf{k}\left\{\mathbf{v}\left(-\frac{df_0}{d\epsilon}\Delta\phi\right)\right\} \tag{5.29a}$$

$$= \frac{e}{4\pi^3}\int d\mathbf{k}\left\{\mathbf{v}\frac{df_0}{d\epsilon}G_0\Omega' G_0 e\mathbf{E}\cdot\mathbf{v}\frac{df_0}{d\epsilon}\right\} \tag{2.29b}$$

This gives us the dot product of $\mathbf{J}_H$ and $e\mathbf{E}'$, where $\mathbf{E}'$ is an electric field chosen as a mathematical tool and has no relation to any electric fields in the physical system.

$$e\mathbf{E}'\cdot\mathbf{J}_H = \frac{e}{4\pi^3}\int d\mathbf{k}\left(-e\mathbf{E}'\cdot\mathbf{v}\frac{df_0}{d\epsilon}\right)G_0\Omega' G_0\left(-e\mathbf{E}\cdot\mathbf{v}\frac{df_0}{d\epsilon}\right) \tag{5.30}$$

It can be seen that by looking at equation (5.22) that the last part of the integrand gives the solution ϕ where no magnetic field is present, ie.,

$$G_0\left(-e\mathbf{E}\cdot\mathbf{v}\frac{df_0}{d\epsilon}\right) = \phi \tag{5.31}$$

Hence, the Hall current equation is now

$$e\mathbf{E}'\cdot\mathbf{J}_H = \frac{e}{4\pi^3}\int d\mathbf{k}\left(-e\mathbf{E}'\cdot\mathbf{v}\frac{df_0}{d\epsilon}\right)G_0\Omega'\phi \tag{5.32}$$

But, G_0 is a symmetrical operator in the sense that

$$\int g(\mathbf{k})G_0 h(\mathbf{k})\ d\mathbf{k} = \int h(\mathbf{k})G_0 g(\mathbf{k})\ d\mathbf{k} \tag{5.33}$$

for any arbitrary functions $\mathbf{g}(\mathbf{k})$, $\mathbf{h}(\mathbf{k})$ (see appendix C). Using this fact, equation (5.32) may be written in the form

$$e\mathbf{E}'\cdot\mathbf{J}_H = \frac{e}{4\pi^3}\int d\mathbf{k}(\Omega'\phi)G_0\left(-e\mathbf{E}'\cdot\mathbf{v}\frac{df_0}{d\epsilon}\right) \tag{5.34}$$

Now, by the same reasoning that lead to equation (5.32), we now have

$$e\mathbf{E}' \cdot \mathbf{J}_H = \frac{e}{4\pi^3} \int \, d\mathbf{k} (\Omega' \phi) \phi' \tag{5.35a}$$

$$= \frac{e}{4\pi^3} \int \phi' \Omega' \phi \, d\mathbf{k} \tag{5.35b}$$

where ϕ' is the solution to the Boltzmann equation in zero magnetic field and with an electric field $\mathbf{E}'$ applied, as given in equation (5.23).

It is important to emphasise the result obtained in equation (5.35). By choosing the electric field to be in the x, y or z directions, the L.H.S. reduces to $e|\mathbf{E}'|J_{Hx}$, $e|\mathbf{E}'|J_{Hy}$ and $e|\mathbf{E}'|J_{Hz}$ respectively, and so all the components of the Hall current can be found from three simple integrals once the zero magnetic field Boltzmann equation has been solved.

Now that we have obtained an expression for the Hall current, by examining equations (5.17) and (5.35) and choosing suitable directions for $\mathbf{E}$, $\mathbf{E}'$ and $\mathbf{B}$, we arrive at the expressions for the non-zero components of the first order conductivity tensor C_{ijk}, ie.

$$\varsigma = \frac{1}{4\pi^3} \int \, d\mathbf{k} \left(\frac{\phi'_y}{E'_y} \right) \frac{\Omega'_z}{B_z} \left(\frac{\phi_z}{E_z} \right) \tag{5.36}$$

and

$$\eta = \frac{1}{4\pi^3} \int \, d\mathbf{k} \left(\frac{\phi'_z}{E'_z} \right) \frac{\Omega'_z}{B_z} \left(\frac{\phi_y}{E_y} \right) \tag{5.37}$$

where ϕ_z is the solution to the BTE with the electric field in the z-direction, $\mathbf{E} = (0, 0, E_z)$, with similar definitions for ϕ_y, ϕ'_z and ϕ'_y. Also, Ω'_z is the magnetic operator with the applied magnetic field $\mathbf{B}$ in the x-direction.

From these expressions for ς and η and equations (5.19) and (5.20), the integrals for the Hall factors can be written down.

$$r_{zyz} = \frac{ne}{4\pi^3 \sigma_z^2} \int \, d\mathbf{k} \left(\frac{\phi'_z}{E'_z} \right) \frac{\Omega'_z}{B_z} \left(\frac{\phi_y}{E_y} \right) \tag{5.38a}$$

$$r_{yzz} = \frac{ne}{4\pi^3 \sigma_z^2} \int d\mathbf{k} \left(\frac{\phi'_y}{E'_y}\right) \frac{\Omega'_z}{B_z} \left(\frac{\phi_z}{E_z}\right) \tag{5.38b}$$

$$r_{zzy} = \frac{ne}{4\pi^3 \sigma_z^2} \int d\mathbf{k} \left(\frac{\phi'_y}{E'_y}\right) \frac{\Omega'_z}{B_z} \left(\frac{\phi_z}{E_z}\right) \tag{5.38c}$$

where n is the electron density,

$$n = \frac{1}{4\pi^3} \int f_0 \, d\mathbf{k} \tag{5.39}$$

and the conductivities are,

$$\sigma_x = -\frac{e}{4\pi^3} \int d\mathbf{k} \left(-\frac{\phi_x}{E_x} \frac{df_0}{d\epsilon}\right) v_x \tag{5.40a}$$

$$\sigma_z = -\frac{e}{4\pi^3} \int d\mathbf{k} \left(-\frac{\phi_z}{E_z} \frac{df_0}{d\epsilon}\right) v_z \tag{5.40b}$$

All the terms in these integrals have been calculated in the previous chapters so we are in a perfect position to calculate very simply the Hall factors.

The method presented here is based on a similar method developed for hopping transport (Butcher and Kumar, 1980).

5.4 . Numerical Calculation

In this section the numerical results are presented for acoustic and polar optic phonon scattering. In the next section some simple analytical results will be derived to compare with the numerical calculations in certain limits.

5.4.1 . Acoustic Phonon Scattering

The first results to be discussed are the simpler acoustic phonon limited Hall factors calculated using the relaxation time approximation and the method described earlier in this chapter.

Figures 5.1 a, b and c show the variation of the Hall factors with temperature. The electron statistics are non-degenerate with the Fermi level well into the band gap.

Figure 5.1a shows r_{zyz}, where the magnetic field is in the growth direction. Here, the Hall factor only shows a small variation with temperature, rising initially as the temperature is increased and then falling again. There are two processes influencing the magnitude of the Hall factor in this case. Firstly, the electrons are moving higher up the band as the temperature is increased into regions where the electron effective mass in the growth direction, m_z^*, is becoming significantly larger and the band is becoming flatter. This effect does not produce such a large variation in the Hall factor as in the following cases, because in this case all the currents are being produced in the plane of the layers and transport through the layers is not so important. However, because the form of the full three dimensional electron distribution function will affect all the transport coefficients in some way, the increase in m_z^* up the band will influence the value of r_{zyz}, but not in an obviously physically interpretable way.

The second process that will affect the value of the Hall coefficient as the temperature is raised is the increase in the scattering. This is due to the increased number of phonons at the higher temperature. Because the relaxation

times at different energies are scaled by an equal amount, thinking of the Hall factor in terms of the scattering factor $r = \frac{<(\tau/m^*)^2>}{<\tau/m^*>^2}$, it can be seen that the top and the bottom of the ratio will change by an equal factor and the change in the scattering will have little effect.

The next graph, figure 5.1b is the variation of r_{yzz} with temperature. Here, the current is in the growth direction and the magnetic field and resulting Hall electric field are in the plane of the superlattice layers. In this case the Hall factor has a value of ≈ 1 for low temperatures and then falls as the temperature is increased.

If we consider a superlattice system with unit current density in the growth direction, as the temperature is increased, the mobility in the growth direction, μ_z decreases due to the increased scattering and also due to the larger average m_z^* for the electrons in the system as the average electron energy increases. To describe the effect of a unit magnetic field in the plane of the superlattice layers, consider the electrons on a constant energy surface with their wavevector $\mathbf{k}$ approximately along the z direction. It is these electrons that contribute most to the transport when the electric field is in the z direction. The magnetic field moves the electrons around the constant energy surface, and the angle that their wavevector rotates by in a typical scattering time τ will be proportional to the cyclotron frequency for these electrons, $\theta \propto \frac{eB}{m_z^*}$. Thus, if we simply assume that the current density $\mathbf{J}$ rotates by this angle, then for small magnetic field $\mathbf{B}$ and hence small θ, the Hall current produced in the plane of the superlattice layers will be proportional to θ.

$$J_H \propto \theta$$

$$J_H \propto \frac{1}{m_z^*} \tag{5.41}$$

Now, the electric field needed in the layers to counter this current will be

inversely proportional to the mobility in the layers.

$$E_H \propto \frac{J_H}{\mu_z} \tag{5.42}$$

and if we use the simplistic expression for the mobility, $\mu_z = \frac{e\tau}{m_z^*}$, then we have

$$E_H \propto \frac{m_z^*}{m_i^*}$$

and hence the relevant Hall factor also behaves as

$$r_{yzz} \propto \frac{m_z^*}{m_z^*} \tag{5.43}$$

This simple arguement shows that the behaviour of r_{yzz} as the temperature is increased is a consequence of the increase in the average value of m_z^*, causing the Hall factor to fall. This effect dominates over the change in the scattering rates as the temperature is increased, and is quite pronounced.

A similar arguement can be used for the case where the Hall field is in the growth direction and the magnetic field and current density are in the layers to give

$$r_{zzy} \propto \frac{m_z^*}{m_z^*} \tag{5.44}$$

This is indeed what the figure 5.1c shows, an increase in the Hall factor as the temperature is increased.

The next results, figures 5.2a, b and c show the variation of the Hall factors as the Fermi level is varied. The temperature is set at 20K, where acoustic phonon scattering would be expected to make a large contribution for pure samples.

These graphs show even more clearly the effects seen in the previous graphs. In these graphs we can say that the features are due to the electrons that contribute to the transport properties having a higher average energy as the Fermi level is increased. The phonon distribution remains unchanged as the

Fermi level is varied, but the average scattering rate is increasing due to the increase in the final density of states as the electron energies are increased.

Figure 5.2a shows r_{xyz} against Fermi level. When the Fermi level is inside the miniband, the Hall factor is close to one. For degenerate statistics, where only the value of the relaxation time at the Fermi level is important, this is what is predicted by simple analytical calculations for the case where the currents are in the plane of the layers (see the last section of this chapter). However, when the statistics are non-degenerate, the Hall factor deviates from one. The reason for this is because the dependence of the relaxation time on energy becomes important and it is in this regime that the actual form of the scattering plays a role in determining the value of the Hall factors.

The graph of r_{yzx} against Fermi level, figure 5.2b shows a constant value when the Fermi level is in the band gap and the electron statistics are non-degenerate. As the Fermi level is moved up through the miniband the Hall factor falls sharply as the effective mass in the growth direction becomes larger for the electrons at the Fermi level.

Figure 5.2c, r_{zxy}, also shows consistent behaviour, with the Hall factor being constant in the non-degenerate Boltzmann regime and then rising sharply as the Fermi level is increased up through the miniband.

The last set of graphs for the acoustic phonon scattering case, figures 5.3a, b and c show the dependence of the Hall factors on the period of the superlattice. The temperature is again set at 20K and the statistics are non-degenerate. As the period is varied, the superlattice is kept symmetric with the width of the well being set equal to the barrier width.

As the superlattice period is increased, the miniband width soon becomes very narrow (figure 3.1) and the effective mass in the growth direction becomes very large for the larger periods. Thus, the effect seen previously is even more pronounced here, with r_{yzx} falling to below 0.1 for a period of 125Å and r_{zxy} rising to above 10.0 for the same period. As before, the Hall factor

r_{zyz} remains close to one throughout, but does not remain exactly one due to the distribution of electrons throughout the miniband and the variation in the scattering rate with electron energy.

The main conclusion of this section is that the dominant factor determining the value of the Hall factors here is the value of the effective mass in the growth direction for the electrons that are contributing to the transport. It is only when electrons from a range of energies contribute, when the statistics are non-degenerate, that the scattering plays a role in determining the Hall factors, and even then the effect is only really observable in the Hall factor that remains close to one, r_{zyz}.

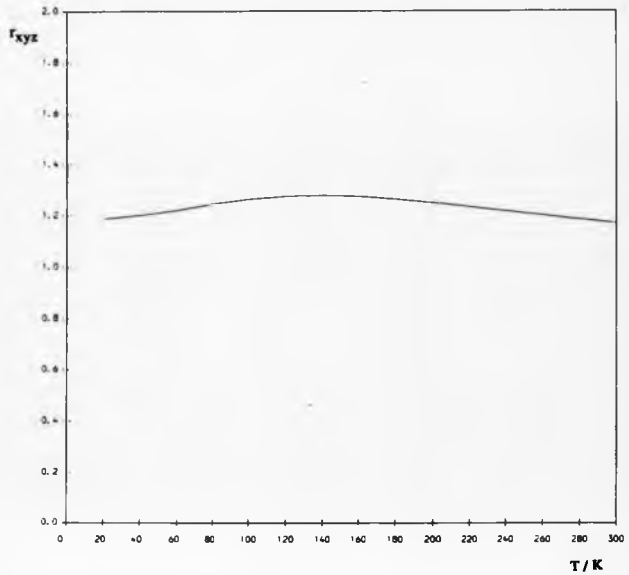

Figure 5.1a: The Hall factor r_{xyz} as a function of temperature. The statistics are Boltzmann and the period is 70Å (well width = barrier width). The scattering is by acoustic phonons.

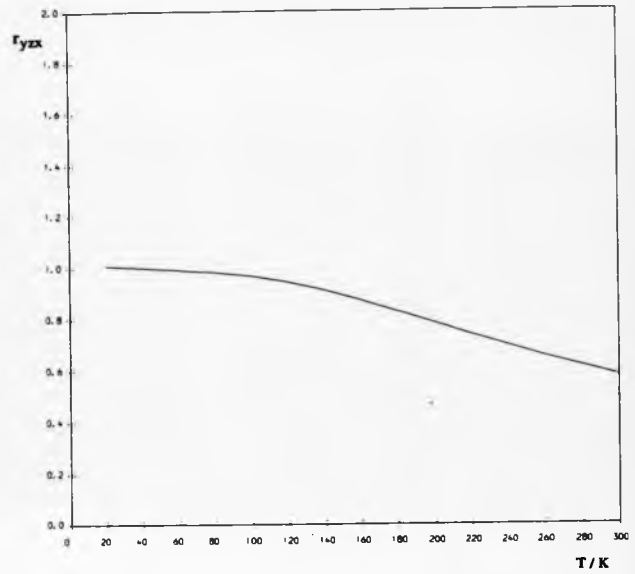

Figure 5.1b: The Hall factor r_{yzx} as a function of temperature. The statistics are Boltzmann and the period is 70Å (well width = barrier width). The scattering is by acoustic phonons.

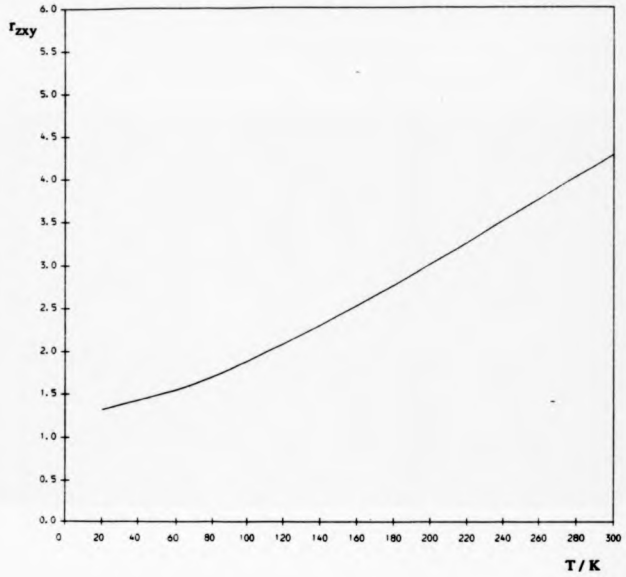

Figure 5.1c: The Hall factor r_{zxy} as a function of temperature. The statistics are Boltzmann and the period is 70Å (well width = barrier width). The scattering is by acoustic phonons.

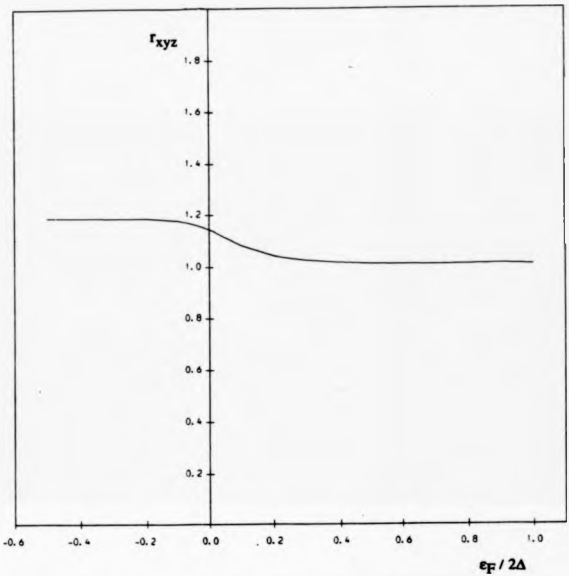

Figure 5.2a: The Hall factor r_{xyz} as a function of Fermi level. The temperature is 20K and the period is 70Å (well width = barrier width). The scattering is by acoustic phonons.

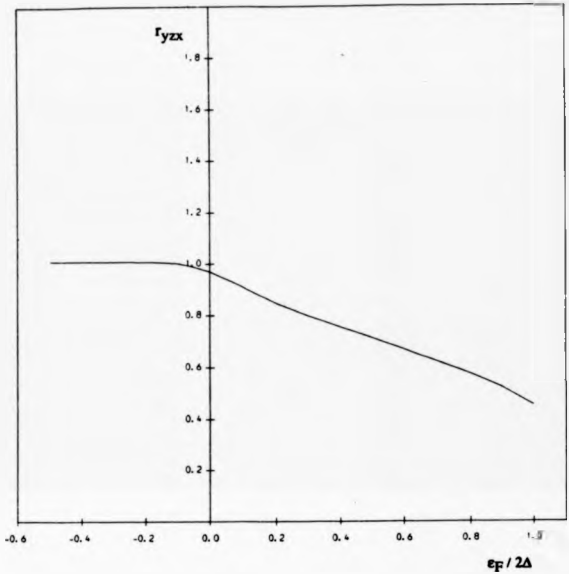

Figure 5.2b: The Hall factor r_{yzx} as a function of Fermi level. The temperature is 20K and the period is 70Å (well width = barrier width). The scattering is by acoustic phonons.

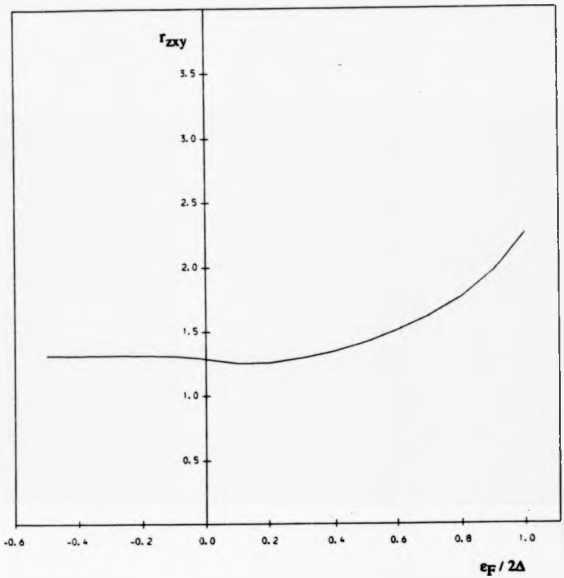

Figure 5.2c: The Hall factor r_{zxy} as a function of Fermi level. The temperature is 20K and the period is 70Å (well width = barrier width). The scattering is by acoustic phonons.

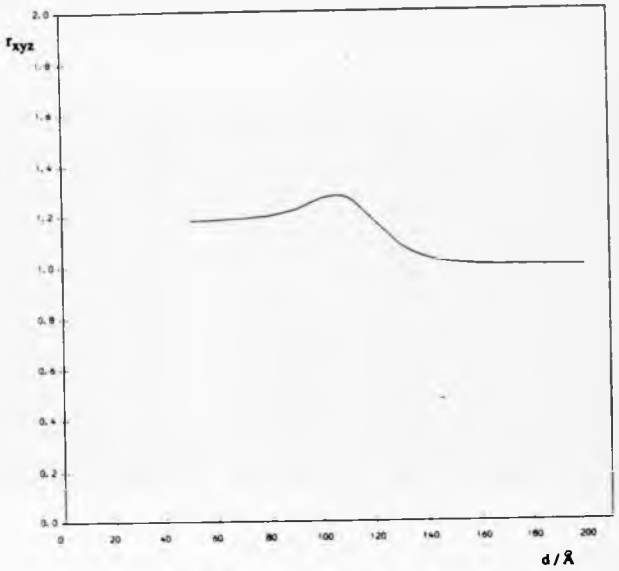

Figure 5.3a: The Hall factor r_{xyz} as a function of superlattice period. The statistics are Boltzmann and the temperature is 20K. The scattering is by acoustic phonons.

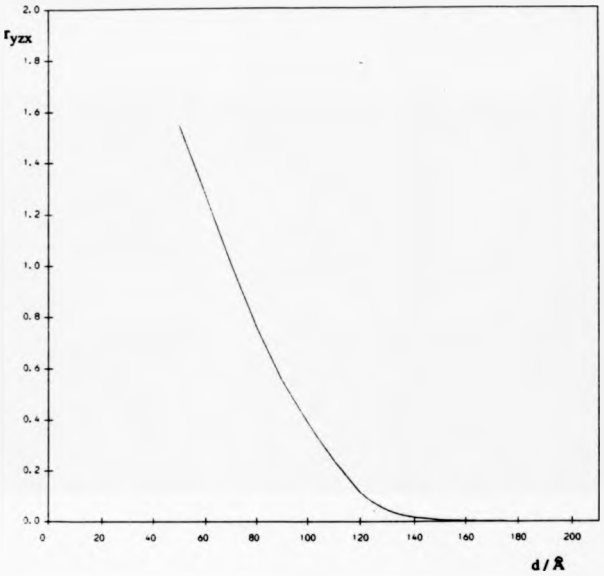

Figure 5.3b: The Hall factor r_{yzx} as a function of superlattice period. The statistics are Boltzmann and the temperature is 20K. The scattering is by acoustic phonons.

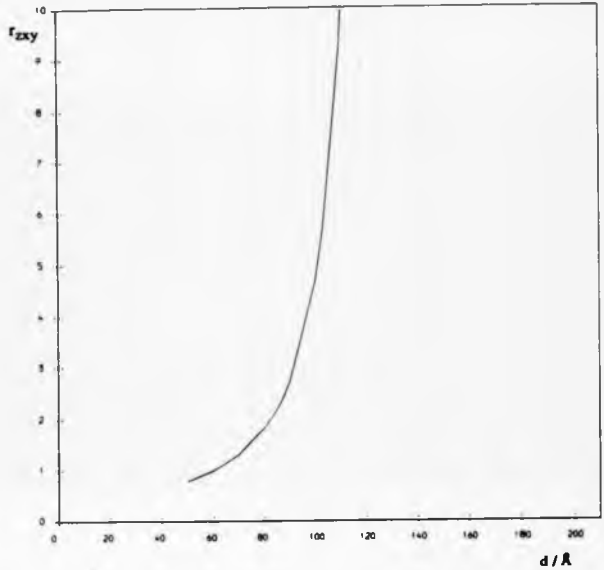

Figure 5.3c: The Hall factor r_{zxy} as a function of superlattice period. The statistics are Boltzmann and the temperature is 20K. The scattering is by acoustic phonons.

5.4.2 . Polar Optic Phonon Scattering

In this section the Hall factor results are presented with polar optic phonon scattering limiting the transport. As for the mobility calculations, the relaxation time approximation is not valid, but the method described in this chapter allows for a simple calculation of the Hall factor results using the distribution function calculated with the iterative technique described in the previous chapters. Results calculated within the relaxation time approximation are also shown to demonstrate the accuracy of this approximation.

In figures 5.4a, b and c is shown the dependence of the Hall factor on the Fermi level. The temperature for these calculations is set at 300K, where polar optic phonon scattering is the dominant scattering mechanism, and the superlattice period is 70Å, with the well width equal to the barrier width.

Figure 5.4a shows r_{zyz} against Fermi level. As for the acoustic phonon calculation, the Hall factor r_{zyz} remains close to 1 as the Fermi level is varied. What the graph does show is that in this case the relaxation time approximation is less accurate in the non-degenerate Boltzmann regime. For r_{zyz}, the anisotropy is not a dominant factor determining the value of the transport parameter because the currents are in the plane of the superlattice layers. So, the effect causing the failure of the relaxation time approximation is the form of the inelastic scattering mechanism. As was found in the previous section, the regime where the form of the scattering has most effect is in the non-degenerate range where the electrons that contribute to the transport are distributed throughout the miniband. This explains why, in this case, the relaxation time approximation breaks down when the electron statistics are non-degenerate but is a reasonable approximation for the degenerate case.

Figure 5.4c, where r_{zzy} is plotted against Fermi level, shows a different behaviour. In this case, the anisotropy of the miniband strongly influences the value of the Hall factor. What is seen now is the failure of the relaxation time approximation for Fermi levels in the non-degenerate and degenerate

regimes. As the Fermi level is moved up through the miniband into energies where the anisotropy is stronger, the disagreement between the relaxation time approximation and the iterative calculation becomes larger.

The third Hall factor r_{yzz} is shown in figure 5.4b. Here we see again the failure of the relaxation time approximation for both non-degenerate and degenerate statistics due to the anisotropy of the miniband and the inelasticity of the scattering mechanism.

The next set of results show the variation of the Hall factors with the superlattice period. The temperature is set at 300K and the statistics are non-degenerate.

A similar dependence on the period is seen here as for the acoustic phonon case. The first graph, figure 5.5a, shows r_{xyz} staying close to 1. The second, figure 5.5b, shows r_{yzz} which becomes smaller as the period is increased and the miniband becomes flatter, with a large effective mass in the growth direction. The third graph, figure 5.5c shows r_{xzy}, which increases as the period and m_z^* increase for the reasons explained earlier in the chapter. In all these graphs, the variations with Fermi level are less pronounced than in the previous section. This is because the higher temperature set in the present calculation gives rise to more thermal broadening in the transport parameters that smooth out the results.

Figures 5.6a,b and c show the final set of results in this section, the variation of the Hall factors with temperature. The statistics are non-degenerate and the superlattice period is 70Å.

These graphs show much the same features as seen in the acoustic phonon case.

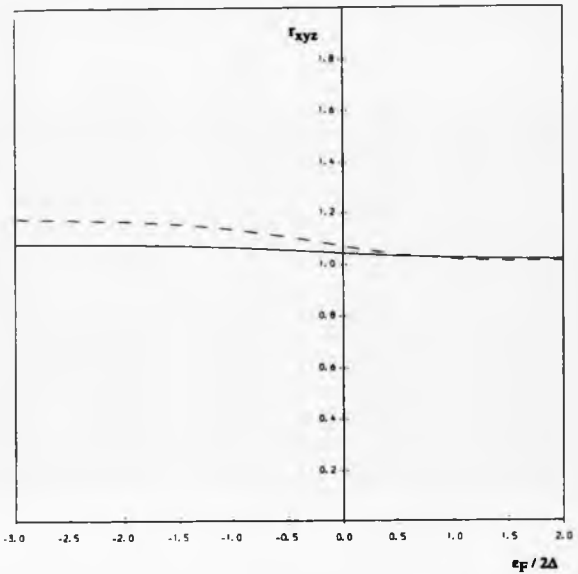

Figure 5.4a: The Hall factor r_{xyz} as a function of Fermi level. The temperature is 300K and the period is 70Å (well width = barrier width). The scattering is by polar optic phonons.

The dashed curve is the relaxation time calculation and the full curve is the iterated solution.

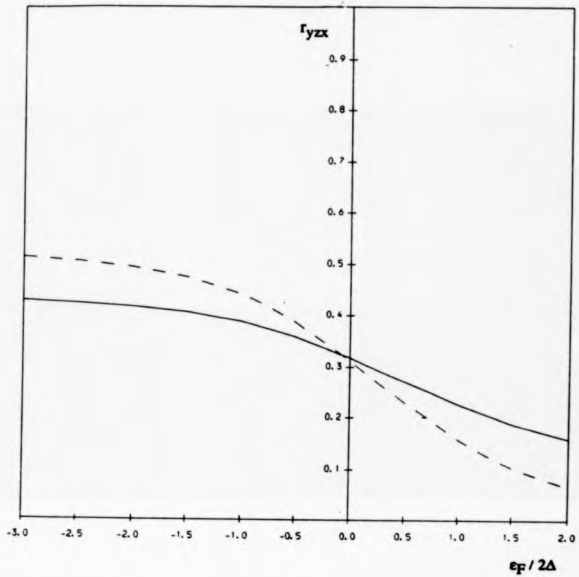

Figure 5.4b: The Hall factor r_{yzx} as a function of Fermi level. The temperature is 300K and the period is 70Å (well width = barrier width). The scattering is by polar optic phonons.

The dashed curve is the relaxation time calculation and the full curve is the iterated solution.

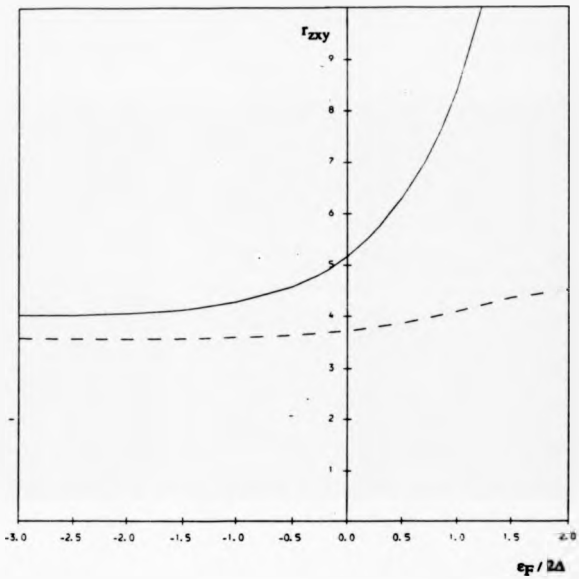

Figure 5.4c: The Hall factor r_{zxy} as a function of Fermi level. The temperature is 300K and the period is 70Å (well width = barrier width). The scattering is by polar optic phonons.

The dashed curve is the relaxation time calculation and the full curve is the iterated solution.

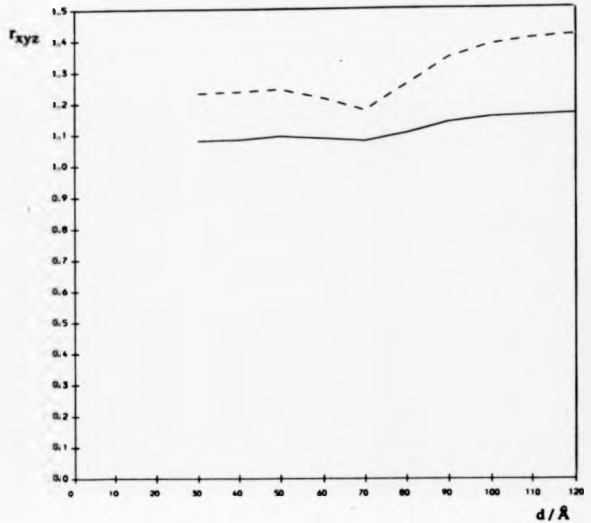

Figure 5.5a: The Hall factor r_{xyz} as a function of superlattice period. The statistics are Boltzmann and the temperature is 300K. The scattering is by polar optic phonons.

The dashed curve is the relaxation time calculation and the full curve is the iterated solution.

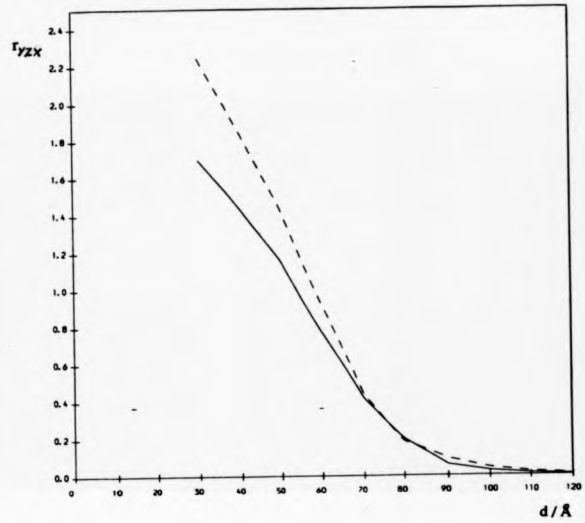

Figure 5.5b: The Hall factor r_{yzx} as a function of superlattice period. The statistics are Boltzmann and the temperature is 300K. The scattering is by polar optic phonons.

The dashed curve is the relaxation time calculation and the full curve is the iterated solution.

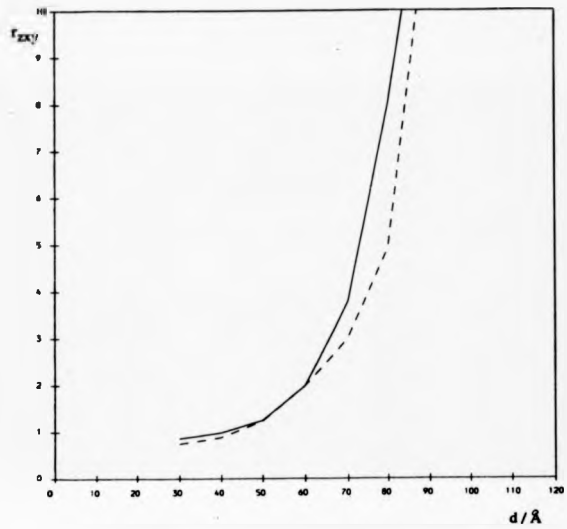

Figure 5.5c: The Hall factor r_{zxy} as a function of superlattice period. The statistics are Boltzmann and the temperature is 300K. The scattering is by polar optic phonons.

The dashed curve is the relaxation time calculation and the full curve is the iterated solution.

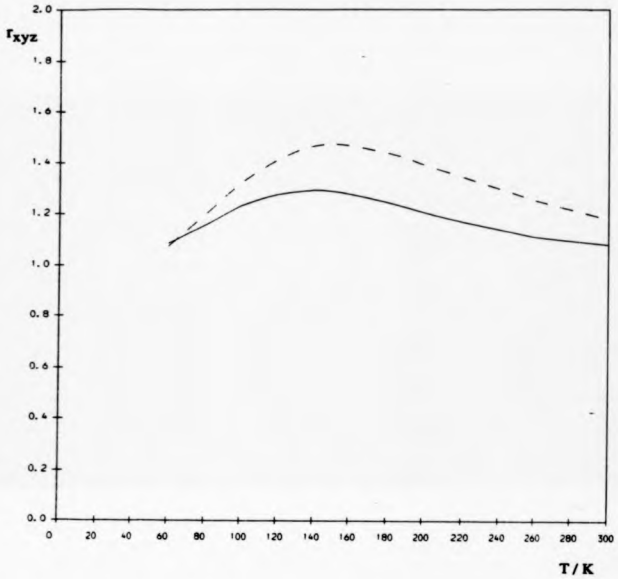

Figure 5.6a: The Hall factor r_{xyz} as a function of temperature. The statistics are Boltzmann and the period is 70Å (well width = barrier width). The scattering is by polar optic phonons.

The dashed curve is the relaxation time calculation and the full curve is the iterated solution.

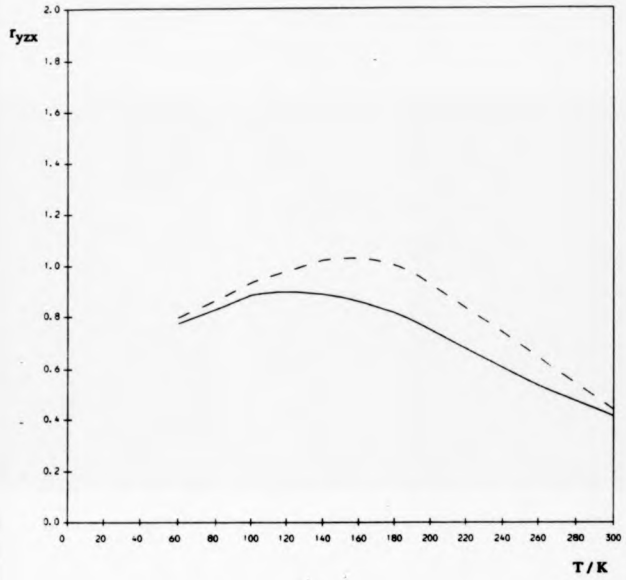

Figure 5.6b: The Hall factor r_{yzx} as a function of temperature. The statistics are Boltzmann and the period is 70Å (well width = barrier width). The scattering is by polar optic phonons.

The dashed curve is the relaxation time calculation and the full curve is the iterated solution.

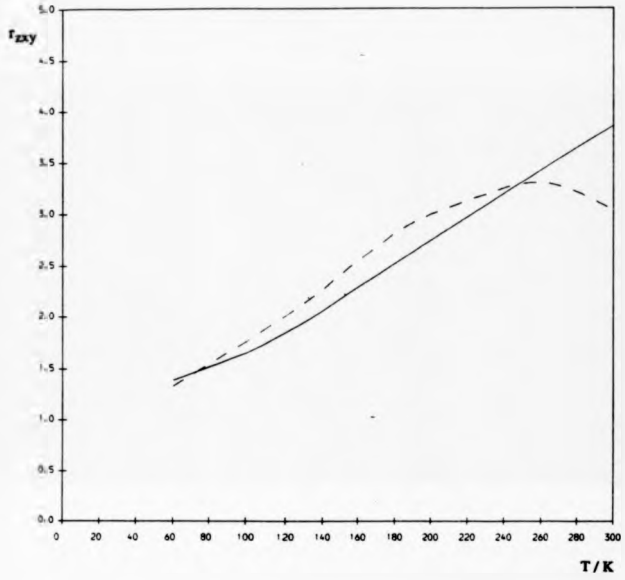

Figure 5.6c: The Hall factor r_{zxy} as a function of temperature. The statistics are Boltzmann and the period is 70Å (well width = barrier width). The scattering is by polar optic phonons.

The dashed curve is the relaxation time calculation and the full curve is the iterated solution.

5.5 . Analytical Limits

In this section the method described at the start of the chapter is used in cases where very simple models are used and many approximations are made. The analytical results that are produced are compared with the numerical results of the previous sections and also with analytical results obtained by other methods.

The simplest approximation to use is to assume that the relaxation time approximation is valid, and that the relaxation time is a constant. In this case, the solution to the linearized Boltzmann equation is simply

$$\phi = -e\mathbf{E}\cdot\mathbf{v}\tau \tag{5.45}$$

From this expression and equation (5.36), the magneto-transport coefficient ς is,

$$\varsigma = -\frac{1}{4\pi^3}\int d\mathbf{k}\,(-ev_y\tau)\left(\frac{df_0}{d\epsilon}\frac{e}{\hbar}v_y\right)\left(-e\tau\frac{\partial v_z}{\partial k_z}\right) \tag{5.46}$$

If we now also assume that the miniband is ellipsoidal and parabolic at the bottom, with effective masses $m_x^* = m_y^*$ and m_z^*, then equation (5.46) simplifies to,

$$\varsigma = -\frac{1}{4\pi^3}\int d\mathbf{k}(-ev_y\tau)\left(\frac{df_0}{d\epsilon}\frac{e}{\hbar}v_y\right)\left(-e\tau\frac{\hbar}{m_z^*}\right) \tag{5.47a}$$

$$= -\frac{e}{4\pi^3}\frac{\tau^2}{m_z^*}\int d\mathbf{k}\left(v_y^2\frac{df_0}{d\epsilon}\right) \tag{5.47b}$$

but, within the approximations assumed here, the conductivities are given by

$$\sigma_x = -\frac{e}{4\pi^3}\tau\int d\mathbf{k}\left(v_x^2\frac{df_0}{d\epsilon}\right) \tag{5.48}$$

with similar expressions for σ_y and σ_z. Thus, from equations (5.47) and (5.48), we have

$$\zeta = \frac{e\tau}{m_y^*}\sigma_y \tag{5.49}$$

and similarly

$$\eta = \frac{e\tau}{m_z^*}\sigma_z \tag{5.50}$$

This leads to,

$$r_{xyz} = \frac{1}{\sigma_x}\frac{ne^2\tau}{m_x^*} \tag{5.51a}$$

$$r_{xzy} = \frac{\sigma_y}{\sigma_x}\frac{ne^2\tau}{m_z^*} \tag{5.51b}$$

$$r_{yzx} = \frac{1}{\sigma_z}\frac{ne^2\tau}{m_y^*} \tag{5.51c}$$

Now, with the simple approximations assumed here, the conductivities are

$$\sigma_i = \frac{ne^2\tau}{m_i^*} \tag{5.52}$$

where $i \equiv x, y, z$. Thus the simple expression arrived at for the Hall factors is,

$$r_{xyz} = 1 \tag{5.53a}$$

$$r_{xzy} = \frac{m_z^*}{m_z^*} \tag{5.53b}$$

$$r_{yzx} = \frac{m_y^*}{m_y^*} \tag{5.53c}$$

This agrees with the simple physical arguement given in section 5.4.1 which arrived at the relationships $r_{zzy} \propto \frac{m_z^*}{m_z^*}$ and $r_{yzz} \propto \frac{m_z^*}{m_z^*}$.

This calculation can now be compared with the acoustic phonon calculation results, seen in figures 5.2a, b and c.

When the Fermi level is in the centre of the miniband, $\epsilon_F = \Delta$, the Hall factor $r_{zyz} = 1.012$, and the product of the other two Hall factors is $r_{yzz} \times r_{zzy} = 1.009$. The actual value of these Hall factors gives an effective mass in the growth direction of $m_z^* = 0.112 m_0$. The relationship $r_{yzz} = 1/r_{zzy}$ does not hold in the Boltzmann regime because, as stated earlier, the scattering becomes important and hence the dependence of the relaxation time on energy becomes important.

Now suppose a relaxation time can be defined that is dependent only on energy, $\tau = \tau(\epsilon)$. Then, the transport parameters are given by,

$$\eta = -\frac{e^3}{4\pi^3\hbar} \int d\mathbf{k} \left\{ v_z^2 \frac{\partial v_y}{\partial k_y} \tau^2(\epsilon) \frac{df_0}{d\epsilon} \right\} \tag{5.54}$$

and

$$\sigma_z = -\frac{e}{4\pi^3} \int d\mathbf{k} \left\{ v_z^2 \tau(\epsilon) \frac{df_0}{d\epsilon} \right\} \tag{5.55}$$

For a system with spherical energy bands, the integrals can be transformed into energy integrals to give,

$$\eta = -\frac{e^3}{4\pi^3} 2\pi \left(\frac{2m_z^*}{\hbar^2} \right)^{3/2} \int_0^\infty \epsilon^{1/2} \, d\epsilon \left\{ v_z^2 \frac{\partial v_y}{\partial k_y} \tau^2(\epsilon) \frac{df_0}{d\epsilon} \right\}$$

$$= -\frac{e^3\hbar}{3\pi^2 m_z^{*2}} \left(\frac{2m_z^*}{\hbar^2} \right)^{3/2} \int_0^\infty \epsilon^{3/2} \tau^2(\epsilon) \frac{df_0}{d\epsilon} \, d\epsilon \tag{5.56}$$

and

$$\sigma_z = -\frac{e^2}{3\pi^2 m_z^*} \left(\frac{2m_z^*}{\hbar^2} \right)^{3/2} \int_0^\infty \epsilon^{3/2} \tau(\epsilon) \frac{df_0}{d\epsilon} \, d\epsilon \tag{5.57}$$

To obtain the Hall factor, the electron density is also needed.

$$
\begin{aligned}
n &= \frac{1}{4\pi^3}\int f_0 d\mathbf{k} \\
&= \frac{1}{2\pi^2}\left(\frac{2m^*}{\hbar^2}\right)^{3/2}\int_0^\infty \epsilon^{1/2} f_0 d\epsilon \qquad (5.58) \\
&= -\frac{1}{3\pi^2}\left(\frac{2m^*}{\hbar^2}\right)^{3/2}\int_0^\infty \epsilon^{3/2}\frac{df_0}{d\epsilon} d\epsilon
\end{aligned}
$$

where the last step is done by integrating by parts. Combining equations (5.56), (5.57) and (5.58) now gives the expression for the Hall factor.

$$
\begin{aligned}
r &= \frac{ne\eta}{\sigma_z^2} \\
&= \frac{\int_0^\infty \epsilon^{3/2}\frac{df_0}{d\epsilon}\, d\epsilon \quad \int_0^\infty \epsilon^{3/2}\tau^2(\epsilon)\frac{df_0}{d\epsilon}\, d\epsilon}{\left[\int_0^\infty \epsilon^{3/2}\tau(\epsilon)\frac{df_0}{d\epsilon}\, d\epsilon\right]^2} \\
&= \frac{<\tau^2>}{<\tau>^2} \qquad (5.59)
\end{aligned}
$$

where the averaging bracket is defined as

$$
<g(\epsilon)> = \frac{\int_0^\infty \epsilon^{3/2} g(\epsilon)\frac{df_0}{d\epsilon}\, d\epsilon}{\int_0^\infty \epsilon^{3/2}\frac{df_0}{d\epsilon}\, d\epsilon} \qquad (5.60)
$$

The expression (5.59) is a standard result produced by conventional relaxation time approximation methods (Smith, Janak and Adler; 1967), and is sometimes called the scattering factor (Butcher, 1973). Thus, a limiting case of the method presented in this chapter reproduces standard relaxation time results as should be expected.

The calculation of the Hall factors that includes the form of the miniband structure given in equation (2.12) is more involved, and can be found in

appendix D. The final result is, for degenerate statistics, a relaxation time dependent on energy alone and a Fermi level within the miniband,

$$r_{zyz} = 1 \tag{5.61a}$$

$$r_{yzz} = \frac{\Delta d^2 m_z^*}{2\hbar^2} \frac{\left\{\left(\frac{\epsilon_F}{\Delta} - 1\right)\left[\frac{\epsilon_F}{\Delta}\left(2 - \frac{\epsilon_F}{\Delta}\right)\right]^{1/2} + \cos^{-1}\left(1 - \frac{\epsilon_F}{\Delta}\right)\right\}}{\left\{\left[\frac{\epsilon_F}{\Delta}\left(2 - \frac{\epsilon_F}{\Delta}\right)\right]^{1/2} + \left(\frac{\epsilon_F}{\Delta} - 1\right)\cos^{-1}\left(1 - \frac{\epsilon_F}{\Delta}\right)\right\}} \tag{5.61b}$$

$$r_{zzy} = r_{yzz}^{-1} \tag{5.61c}$$

Again, using the acoustic phonon case as an example, where the relaxation time is dependent on energy alone, the value of r_{yzz} when the Fermi level is in the centre of the miniband is $r_{yzz} = 0.712$, which compares well with the value given by equation (5.61) of $r_{yzz} = 0.714$. The values for r_{zzy} are 1.42 from the numerical calculation and 1.40 from the analytical expression.

As a final simple calculation, consider the polar optic case where the statistics are non-degenerate. A relaxation time cannot strictly be defined, but for simple calculations a relaxation time is commonly taken to be of the form (Nag, 1972; Smith, Janak and Adler, 1967)

$$r_{PO}(\epsilon) \sim \epsilon^{1/2} \tag{5.62}$$

Now, for Boltzmann statistics, the electrons are at the bottom of the band, so the form of the miniband will be assumed to be parabolic, and so equation (5.59) is used to calculate r_{zyz}.

With the form of the relaxation time in equation (5.62) and for Boltzmann statistics, i.e.

$$\frac{df_0}{d\epsilon} \simeq -\beta e^{-\beta\epsilon} \tag{5.63}$$

the expression for the Hall factor reduces to

$$r_{xyz} = \frac{\int_0^\infty \epsilon^{3/2} e^{-\beta\epsilon}\, d\epsilon \int_0^\infty \epsilon^{3/2} e^{-\beta\epsilon}\, d\epsilon}{\left[\int_0^\infty \epsilon^{2} e^{-\beta\epsilon}\, d\epsilon\right]^2} \tag{5.64}$$

These integrals are standard, and the result is,

$$r_{xyz} = \frac{45\pi}{128}$$

$$\simeq 1.10$$

This shows that the scattering in the polar optic case increases the value of the Hall factor above 1, and this is the effect seen in figure 5.4a.

CHAPTER 6

CONCLUSIONS

6.1 . Mobility Calculation

The mobility is probably the easiest transport parameter to understand physically, being the average drift velocity of the charge carriers per unit electric field. This made the interpretation of the results in relation to the superlattice structure more straightforward.

The behaviour of the mobility as the temperature is varied was very simple to interpret. As the temperature increases, the amount of phonon scattering increases, limiting the motion of the electrons, and so the mobility falls. These results display no strong features that can be attributed to the small scale structure of the system.

In both the acoustic phonon case and the polar optic phonon case, the rapid fall of μ_z as the period is increased was observed as expected. The wide barriers impede the motion of the electrons and only a small amount of tunneling through the barrier layers occurs. The behaviour of $\mu_{||}$ in the acoustic case is easily interpreted by using a simple analytical calculation with a constant relaxation time, which is a good approximation in some regimes (ie. when the miniband is narrow, and the D.O.S. is a constant for most energies). This calculation describes the behaviour when it is applicable, and where the energy dependence of the relaxation time becomes important, simple arguments can be made as to how the mobility will be modified.

The variation of the mobilities μ_z and $\mu_{||}$ with Fermi level show clear effects that result from the superlattice structure. As the Fermi level moves above the top of the miniband and the D.O.S. becomes constant, clear changes in the behaviour of the mobility curve can be seen.

For the polar optic phonon case, an important point to note is the size of the discrepency between the simple relaxation time approximation calculation and the exact iterative solution. There is a large difference in the value of the mobility obtained by the two methods, the difference being as large as a factor of about two in some cases. This shows that the combination of the inelasticity of the scattering and the anisotropy of the miniband structure must be taken into account when calculating the transport coefficients.

6.2 . Thermopower Calculation

In the Boltzmann regime, the thermopower is always accurately described by equation (3.26) as the electron energies are far away from the Fermi level. Thus the interesting features are seen for degenerate statistics when the Fermi level is within the miniband, or above the top of the miniband.

One of the most prominent features in the acoustic phonon results is the positive peak in S_z as the Fermi level passes the top of the miniband. This peak is a direct result of the form of the superlattice miniband structure. Positive peaks in the thermopower have also be predicted in quasi-1D and quasi-2D systems. Another consequence of the miniband structure is the difference in the magnitude of $S_\parallel$ and S_z by a factor of about two. This was illustrated by a simple analytic calculation assuming a constant relaxation time. The thermopower results for the polar optic phonon case do not show the positive peak in the thermopower due to the increased thermal broadening at the higher temperature set for the calculation. However, the difference in the magnitude of $S_\parallel$ and S_z is still present, demonstrating the effect of the superlattice structure.

6.3 . Hall Factor Calculation

The Hall factor results are interesting in that they can give a direct indication of the form of the miniband structure under certain conditions. In the case of degenerate statistics, the actual form of the scattering has little effect,

especially at low temperatures where the elastic acoustic phonon scattering will be stronger than the inelastic polar optic phonon scattering. In this situation, the Hall factors r_{yzz} and r_{zzy} give the ratio of the effective masses in the growth direvtion and in the direction parallel to the layers. The other Hall factor, r_{xyz}, should give a value close to one, and will indicate how much effect the scattering is having by how far it deviates from one.

The polar optic phonon calculation is interesting because the effect of the inelastic scattering and the anisotropic miniband structure on the accuracy of the relaxation time approximation can be looked at individually. The Hall factor r_{xyz} is not affected strongly by the anisotropy, and thus can be used to study the effect of the scattering. It shows that the relaxation time approximation approximation fails for Boltzmann statistics but is accurate for degenerate statistics. This is because the energy variation of the scattering is important for Boltzmann statistics, where the electrons contributing to transport are distributed throughout the miniband. So, if we now look at the other two Hall factors in the degenerate regime, this will give an indication of how much the anisotropy affects the validity of the relaxation time approximation. Figures 5.4b and 5.4c show that the anisotropy does indeed have a large effect and the relaxation time approximation cannot be used for degenerate statistics.

6.4 . Summary

The object of this thesis has been to show the effect of the small scale structure of a superlattice on the transport propreties. In each chapter, results were presented for both acoustic phonon limited transport and polar optic phonon limited transport. The acoustic phonon calculation is the simplest, where the relaxation time approximation holds. This was used to gain an insight into the behaviour of the electrons in the superlattice under various conditions. The polar optic calculation was more involved, and two methods were used. The simple relaxation time approximation, which is not valid for

this case, and the iterative approach. The iterative is the exact calculation and the relaxation time method was used to demonstrate its own failings due to the inelasticity of the scattering and the anisotropy of the miniband structure. This was shown particularly clearly in the Hall factor calculation. In this calculation, regimes could be found where either the scattering or the miniband structure dominated the results, and the effect of each could be looked at individually.

Finally, the method used for the Hall factor calculations is as important as the results themselves. This is a novel method and could be used for many other systems. It is particularly useful if the relaxation time approximation is not valid and the Jones-Zener expansion cannot be used. Using this method, little further work is needed if the zero magnetic field Boltzmann equation has been solved for the system in question.

APPENDIX A

Symmetry of the Transport Tensors σ_{ij} and C_{ijk}

In the effective mass approximation, a superlattice has all the symmetry of the crystal point group 4/mmm, ie. a fourfold rotation axis and three mirror planes.

$$4_z \quad : \quad \begin{pmatrix} 0 & 1 & 0 \\ -1 & 0 & 0 \\ 0 & 0 & 1 \end{pmatrix}$$

$$m_z \quad : \quad \begin{pmatrix} 1 & 0 & 0 \\ 0 & 1 & 0 \\ 0 & 0 & -1 \end{pmatrix}$$

$$m_x \quad : \quad \begin{pmatrix} -1 & 0 & 0 \\ 0 & 1 & 0 \\ 0 & 0 & 1 \end{pmatrix}$$

$$m_{(110)} \quad : \quad \begin{pmatrix} 0 & 1 & 0 \\ 1 & 0 & 0 \\ 0 & 0 & 1 \end{pmatrix}$$

The transport tensors σ_{ij} and C_{ijk} transform in the standard way when considering a symmetry operator l_{ij}.

$$\sigma_{ij} = l_{ik} l_{jl} \sigma_{kl} \tag{A1a}$$

$$C_{ijk} = \frac{l_{il} l_{jm} l_{kn}}{|l|} C_{lmn} \tag{A1b}$$

If the conductivity tensor σ_{ij} is transformed under the operation of of the mirror plane m_x, it follows that,

$$\sigma_{12} = (-1)(+1)\sigma_{12} = -\sigma_{12} = 0 \tag{A2}$$

Similarly, it can be shown that the only non-zero components are those with repeated indices, and these can be represented by two parameters.

$$\sigma_{11} = \sigma_{22} = \sigma_{\parallel} \tag{A3a}$$

$$\sigma_{33} = \sigma_z \tag{A3b}$$

For C_{ijk}, the transformation under the operation of the the mirror plane m_z produces the result

$$C_{113} = \frac{(-1)(-1)(+1)}{(-1)} C_{113} = -C_{113} = 0 \tag{A4}$$

Similarly, any component with repeated indices will be zero. For the remaining six terms, operating with the rotation axis 4_z gives,

$$C_{123} = -\,C_{213} \tag{A4a}$$

$$C_{231} = -\,C_{132} \tag{A4b}$$

$$C_{321} = -\,C_{312} \tag{A4c}$$

Finally, the conductivity tensor has Onsager symmetry.

$$\sigma_{ij}(\mathbf{B}) = \sigma_{ji}(-\mathbf{B}) \tag{A5}$$

where

$$\sigma_{ij}(\mathbf{B}) = \sigma_{ij}(0) + C_{ijk}B_k + d_{ijkl}B_kB_l + \cdots \tag{A6}$$

Therefore it is also true that,

$$\sigma_{ji}(-\mathbf{B}) = \sigma_{ji}(0) - C_{jik}B_k + d_{jikl}B_kB_l + \cdots \tag{A7}$$

Comparing equations (A5), (A6) and (A7) gives

$$C_{ijk} = -C_{jik} \tag{A8}$$

So, using this result along with the relations in equation (A4) the tensor C_{ijk} can be expressed with just two independent parameters.

$$C_{123} = -C_{213} = \epsilon \tag{A9a}$$

$$C_{231} = C_{312} = -C_{321} = -C_{132} = \varsigma \tag{A9b}$$

APPENDIX B

Form of $g_i(\mathbf{k})$ when the applied electric field is parallel to the layers

For polar optic phonon scattering, the iterative equation for $g(\mathbf{k})$ is

$$g_{i+1}(\mathbf{k}) = \frac{\gamma \int_0^{2\pi} d\theta' \int_{\Gamma^+} dk'_z \; g_i(\mathbf{k}') \left\{ \frac{(1-f_0(\mathbf{k}))[N+1/2\pm1/2]+f_0(\mathbf{k})[N+1/2\pm1/2]}{|\mathbf{k}-\mathbf{k}'|^2} \right\} - \frac{1}{\hbar}\mathbf{E}\cdot\nabla_{\mathbf{k}} f_0}{\gamma \int_0^{2\pi} d\theta' \int_{\Gamma^+} dk'_z \left\{ \frac{(1-f_0(\mathbf{k}'))[N+1/2\pm1/2]+f_0(\mathbf{k}')[N+1/2\mp1/2]}{|\mathbf{k}-\mathbf{k}'|^2} \right\}} \tag{B1}$$

where γ and N are constants, and the limits $\Gamma^{\pm}$ are given in table 3.1. The Fermi-Dirac distribution function $f_0(\mathbf{k})$ is independent of θ, ie. $f_0(\mathbf{k}) = f_0(k_{\parallel}, k_z)$ where $k_{\parallel} = (k_x^2 + k_y^2)^{1/2}$.

For $\mathbf{E} = (E, 0, 0)$,

$$\begin{aligned}
\mathbf{E}\cdot\nabla_{\mathbf{k}} f_0 &= E\frac{\partial f_0}{\partial k_x} \\
&= E\frac{df_0}{d\varepsilon}\frac{\partial \varepsilon}{\partial k_x} \\
&= -E\beta f_0(1-f_0)\frac{\hbar^2}{m_z^*}k_z \\
&= -E\beta f_0(1-f_0)\frac{\hbar^2}{m_z^*}k_{\parallel}\cos\theta
\end{aligned} \tag{B2}$$

Therefore, the first iteration is proportional to $\cos\theta$, and can be written in the form,

$$g_1(\mathbf{k}) = \tilde{g}_1(k_{\parallel}, k_z)\cos\theta \tag{B3}$$

Hence, the upper integral for the second iteration is,

$$I = \int_0^{2\pi} d\theta' \int_{\Gamma\pm} dk_z' \left\{ \frac{\tilde{g}_1(k_\parallel', k_z') \cos\theta' F(k_\parallel, k_z)}{k_\parallel'^2 + k_\parallel^2 + (k_z' - k_z)^2 - 2k_\parallel' k_\parallel \cos(\theta - \theta')} \right\} \qquad (B4)$$

where

$$F(k_\parallel, k_z) = (1 - f_0)[N + 1/2 \mp 1/2] + f_0[N + 1/2 \pm 1/2] \qquad (B5)$$

The order of integration can now be reversed as the k_z' limits are independent of θ', and the integral can be written in the more transparent form,

$$I = \int_{\Gamma\pm} dk_z' \int_0^{2\pi} d\theta' \left\{ \frac{A \cos\theta'}{b - c\cos(\theta - \theta')} \right\} \qquad (B6)$$

where

$$A = \tilde{g}_1(k_\parallel', k_z') F(k_\parallel, k_z) \qquad (B7a)$$

$$b = k_\parallel'^2 + k_\parallel^2 + (k_z' - k_z)^2 \qquad (B7b)$$

$$c = 2k_\parallel' k_\parallel \qquad (B7c)$$

A simple change of variables transforms the integral into,

$$I = \int_{\Gamma\pm} dk_z' \int_0^{2\pi} d\theta'' \left\{ \frac{A\cos(\theta'' + \theta)}{b - c\cos\theta''} \right\}$$

$$= \int_{\Gamma\pm} dk_z' \int_0^{2\pi} d\theta'' \left\{ \frac{A\cos\theta''\cos\theta - A\sin\theta''\sin\theta}{b - c\cos\theta''} \right\} \qquad (B8)$$

Since $\frac{\sin\theta''}{b - c\cos\theta''}$ is antisymmetrical about $\theta'' = \pi$, that part of the integral vanishes, and the integral reduces to,

$$I = \cos\theta \times \int_{\Gamma\pm} dk_z' \int_0^{2\pi} d\theta'' \left\{ \frac{A\cos\theta''}{b - c\cos\theta''} \right\} \qquad (B9)$$

Therefore, $I \propto \cos\theta$, and thus $g_2(\mathbf{k}) \propto \cos\theta$. So, by induction, it must also be true that g_3, g_4, g_5 etc are also proportional to $\cos\theta$. And so, the iterative equation for $g(\mathbf{k})$ with the applied electric field in the plane of the superlattice layers can be written in the form,

$$\tilde{g}_{i+1} = \frac{2\pi\gamma \int_{\Gamma^+} dk_x' \left\{ \frac{\vec{k}\cdot\vec{F}}{c} \left[\frac{b}{(b^2-c^2)^{1/2}} - 1 \right] \right\} + \frac{e}{\hbar} E\beta f_0(1-f_0) \frac{\hbar^3}{m_{\parallel}^* c} k_{\parallel}}{2\pi\gamma \int_{\gamma^+} dk_x' \left\{ \frac{(1-f_0')[N+1/2+1/2]+f_0'[N+1/2+1/2]}{(b^2-c^2)^{1/2}} \right\}} \tag{B10}$$

and

$$g_i(\mathbf{k}) = \tilde{g}_i(k_{\parallel}, k_x) \cos\theta \tag{B11}$$

APPENDIX C

Symmetry of G_0

It has been shown previously by simple arguements (Butcher, 1973) that the collision operator C is symmetrical in an integral, ie.,

$$\int g(\mathbf{k}) C h(\mathbf{k})\ d\mathbf{k} = \int h(\mathbf{k}) C g(\mathbf{k})\ d\mathbf{k} \tag{C1}$$

where g(k) and h(k) are arbitrary functions of k. Now, let us define some new functions such that,

$$g(\mathbf{k}) = C^{-1} l(\mathbf{k}) \tag{C2a}$$

$$h(\mathbf{k}) = C^{-1} m(\mathbf{k}) \tag{C2b}$$

Inserting these definitions into equation (C1) gives

$$\int (C^{-1} l)\mathbf{k})) C C^{-1} m(\mathbf{k})\ d\mathbf{k} = \int (C^{-1} m(\mathbf{k})) C C^{-1} l(\mathbf{k})\ d\mathbf{k} \tag{C3}$$

Thus, putting $G_0 = C^{-1}$,

$$\int m(\mathbf{k}) G_0 l(\mathbf{k})\ d\mathbf{k} = \int l(\mathbf{k}) G_0 m(\mathbf{k})\ d\mathbf{k} \tag{C4}$$

and G_0 is also symmetric.

APPENDIX D

Analytic Calculation of the Hall Factors for a Special Case

The calculation here gives an analytical expression for the Hall factors when the following approximations are used.

(i) The relaxation time is a function of energy only, $\tau \equiv \tau(\epsilon)$.

(ii) The statistics are degenerate.

(iii) The miniband structure is

$$\epsilon(\mathbf{k}) = \frac{\hbar^2 k_\perp^2}{2m_z^*} + \Delta(1 - \cos k_z d)$$

With a relaxation time $\tau(\epsilon)$ defined, the solution to the Boltzmann equation is,

$$\phi = -e\mathbf{E} \cdot \mathbf{v} \frac{df_0}{d\epsilon} \tau(\epsilon) \qquad (D1)$$

Inserting this solution into equations (5.36), (5.37) and (5.40) gives us the expressions for ς, η, σ_x, σ_y and σ_z.

$$\varsigma = -\frac{e^3}{4\pi^3\hbar} \int d\mathbf{k} \left\{ v_y^2 \frac{\partial v_x}{\partial k_x} \tau^2(\epsilon) \frac{df_0}{d\epsilon} \right\} \qquad (D2)$$

$$\eta = -\frac{e^3}{4\pi^3\hbar} \int d\mathbf{k} \left\{ v_x^2 \frac{\partial v_y}{\partial k_y} \tau^2(\epsilon) \frac{df_0}{d\epsilon} \right\} \qquad (D3)$$

$$\sigma_x = \sigma_y = -\frac{e^2}{4\pi^3} \int d\mathbf{k} \left\{ v_x^2 \tau(\epsilon) \frac{df_0}{d\epsilon} \right\} \qquad (D4)$$

$$\sigma_z = -\frac{e^2}{4\pi^3} \int d\mathbf{k} \left\{ v_z^2 \tau(\epsilon) \frac{df_0}{d\epsilon} \right\} \qquad (D5)$$

For the degenerate case, with the Fermi level at the energy ϵ_F, the integral for ς reduces to,

$$\varsigma = \frac{e^3}{4\pi^3\hbar} \int k_{\|}\ dk_{\|} d\theta dk_z \left\{ \left(\frac{\hbar k_{\|}}{m_z^*} \sin\theta \right)^2 \frac{\Delta d}{\hbar} \cos k_z d\ \ \tau^2(\epsilon) \delta(U) \right\} \qquad (D6)$$

$$= \frac{e^3 m_z^*}{4\pi^3\hbar^2} \tau^2(\epsilon_F) \int_0^{2\pi} \sin^2\theta\ d\theta \int d\left(\frac{\hbar^2 k_{\|}^2}{2m_z^*} \right)\ dk_z \left\{ \frac{\hbar^2 k_{\|}^2}{m_z^{*2}} \frac{\Delta d^2}{\hbar} \cos k_z d\ \delta(U) \right\}$$

where $U = \frac{\hbar^2 k_{\|}^2}{2m_z^*} + \Delta(1 - \cos k_z d) - \epsilon_F$.

The θ-integral is simple, and the $k_{\|}$ integral follows from the properties of the δ-function to give

$$\varsigma = \frac{e^3 \Delta d^2 \tau^2(\epsilon)}{2\pi^2\hbar^4} \int_{-k_1}^{k_1} dk_z \left\{ (\epsilon_F - \Delta(1 - \cos k_z d)) \cos k_z d \right\} \qquad (D7)$$

where k_1 is the maximum value of k_z on the energy surface $\epsilon = \epsilon_F$. The k_z integral is straightforward, and the result is,

$$\varsigma = \frac{e^3 \Delta d^2 \tau^2(\epsilon_F)}{2\pi^2\hbar^4} \left(\frac{2(\epsilon_F - \Delta)}{d} \sin k_1 d + \frac{\Delta}{2d} \sin 2k_1 d + k_1 \Delta \right) \qquad (D8)$$

with

$$k_1 d = \cos^{-1}\left(1 - \frac{\epsilon_F}{\Delta}\right) \qquad ;\ \epsilon_F < 2\Delta$$

$$= \pi \qquad ;\ \epsilon_F \geq 2\Delta \qquad (D9)$$

Inserting the value of k_1 into equation (D8) gives

$$\varsigma = \frac{e^3 \Delta^2 d\tau^2(\epsilon_F)}{2\pi^2\hbar^4} \left\{ \cos^{-1}\left(1 - \frac{\epsilon_F}{\Delta}\right) - \left(1 - \frac{\epsilon_F}{\Delta}\right) \left[\frac{\epsilon_F}{\Delta} \left(2 - \frac{\epsilon_F}{\Delta}\right) \right]^{1/2} \right\} \qquad ;\ \epsilon_F < 2\Delta$$

$$= \frac{e^3 \Delta^2 d\tau^2(\epsilon_F)}{2\pi\hbar^4} \qquad ;\ \epsilon_F \geq 2\Delta \qquad (D10)$$

A similar calculation gives

$$\eta = \frac{e^3\Delta\tau^2(\epsilon_F)}{\pi^2\hbar^2 m_z^* d}\left\{\left[\frac{\epsilon_F}{\Delta}\left(2-\frac{\epsilon_F}{\Delta}\right)\right]^{1/2} + \left(\frac{\epsilon_F}{\Delta}-1\right)\cos^{-1}\left(1-\frac{\epsilon_F}{\Delta}\right)\right\} \quad ; \ \epsilon_F < 2\Delta$$

$$= \frac{e^3\Delta\tau^2(\epsilon_F)}{\pi\hbar^2 m_z^* d}\left(\frac{\epsilon_F}{\Delta}-1\right) \quad ; \ \epsilon_F \geq 2\Delta \quad (D11)$$

and for σ_x and σ_z, the results are

$$\sigma_z = \frac{e^3\Delta\tau(\epsilon_F)}{\pi^2\hbar^2 d}\left\{\left[\frac{\epsilon_F}{\Delta}\left(2-\frac{\epsilon_F}{\Delta}\right)\right]^{1/2} + \left(\frac{\epsilon_F}{\Delta}-1\right)\cos^{-1}\left(1-\frac{\epsilon_F}{\Delta}\right)\right\} \quad ; \ \epsilon_F < 2\Delta$$

$$= \frac{e^3\Delta\tau(\epsilon_F)}{\pi\hbar^2 d}\left(\frac{\epsilon_F}{\Delta}-1\right) \quad ; \ \epsilon_F \geq 2\Delta \quad (D12)$$

and

$$\zeta = \frac{e^2\Delta^2 dm_x^*\tau(\epsilon_F)}{2\pi^2\hbar^4}\left\{\cos^{-1}\left(1-\frac{\epsilon_F}{\Delta}\right) - \left(1-\frac{\epsilon_F}{\Delta}\right)\left[\frac{\epsilon_F}{\Delta}\left(2-\frac{\epsilon_F}{\Delta}\right)\right]^{1/2}\right\} \quad ; \ \epsilon_F < 2\Delta$$

$$= \frac{e^2\Delta^2 dm_x^*\tau(\epsilon_F)}{2\pi\hbar^4} \quad ; \ \epsilon_F \geq 2\Delta \quad (D13)$$

The only other parameter needed before the Hall factors can be calculated is the electron density. This is given by,

$$n = \frac{1}{4\pi^3}\int f_0 \, d\mathbf{k} \quad (D14)$$

For degenerate statistics, this is

$$n = \frac{1}{4\pi^3}\int_{\epsilon\leq\epsilon_F} d\mathbf{k} \quad (D15)$$

and some straightforward integration gives

$$n = \frac{m_z^* \Delta}{\pi^2 \hbar^2 d} \left\{ \left[\frac{\epsilon_F}{\Delta} \left(2 - \frac{\epsilon_F}{\Delta} \right) \right]^{1/2} + \left(\frac{\epsilon_F}{\Delta} - 1 \right) \cos^{-1} \left(1 - \frac{\epsilon_F}{\Delta} \right) \right\} \quad ; \ \epsilon_F < 2\Delta$$

$$= \frac{m_z^* \Delta}{\pi \hbar^2 d} \left(\frac{\epsilon_F}{\Delta} - 1 \right) \quad ; \ \epsilon_F \geq 2\Delta \qquad (D16)$$

From these expressions, the Hall factors follow.

For $\epsilon_F < 2\Delta$

$$r_{zyz} = \frac{ne\eta}{\sigma_z^2} = 1 \qquad (D17)$$

$$r_{yzz} = \frac{ne\zeta}{\sigma_z^2} \qquad (D18)$$

$$= \frac{\Delta d^2 m_z^*}{2\hbar^3} \frac{\left\{ \cos^{-1} \left(1 - \frac{\epsilon_F}{\Delta} \right) - \left(1 - \frac{\epsilon_F}{\Delta} \right) \left[\frac{\epsilon_F}{\Delta} \left(2 - \frac{\epsilon_F}{\Delta} \right) \right]^{1/2} \right\}}{\left\{ \left[\frac{\epsilon_F}{\Delta} \left(2 - \frac{\epsilon_F}{\Delta} \right) \right]^{1/2} + \left(\frac{\epsilon_F}{\Delta} - 1 \right) \cos^{-1} \left(1 - \frac{\epsilon_F}{\Delta} \right) \right\}}$$

and

$$r_{zzy} = \frac{ne\zeta}{\sigma_z^2} = r_{yzz}^{-1} \qquad (D19)$$

For $\epsilon_F \geq 2\Delta$, the results are

$$r_{zyz} = 1 \qquad (D20)$$

$$r_{yzz} = \frac{\Delta d^2 m_z^*}{2\hbar^2} \left(\frac{\epsilon_F}{\Delta} - 1 \right)^{-1} \qquad (D21)$$

$$r_{zzy} = r_{yzz}^{-1} \qquad (D22)$$

REFERENCES

ABSTREITER, G., BRUGGER, H., WOLF, T., JORKE, H. and HERTZOG, H.J., (1984), *Phys. Rev. Lett.*, **54**, 2441

ANDO, T., FOWLER, A.B. and STERN, F., (1982), *Rev. Mod. Phys.*, **54**, 437

ARTAKI, M. and HESS K., (1985), *Superlattices and Microstructures*, **1**, 6, 489

BARDEEN, J. and SHOCKLEY, W., (1950), *Phys. Rev.*, **80**, 72

BASTARD, G.,(1981), *Phys. Rev. B.*, **24**, 10, 5693

BASTARD, G.,(1982), *Phys. Rev. B.*, **25**, 7584

BLATT, F.,(1968), *Physics of electronic conduction in solids. (McGraw-Hill)*

BUTCHER, P.N.,(1973), *Electrons in Crystalline Solids (Vienna: IAEA)*, p.103

BUTCHER, P.N. and KUMAR, A.A.,(1980), *Phil. Mag. B*, **42**, 201

BUTCHER, P.N., (1985) in *Crystalline Semiconducting Materials and Devices*, (Eds. P.N.Butcher, N.H.March and M.P.Tosi), (Plenum)

CALECKI, D., PALMIER, J.F. and CHOMETTE, A., (1984), *J. Phys. C*, **17**, 5017

CANTRELL, D.G. and BUTCHER, P.N., (1985), *J. Phys. C*, **18**, L587

CHANG, L.L., ESAKI, L., HOWARD, W.E. and LUDEKE, R.,(1973), *J. Vac. Sci. Technol.*, **10**, 11

CHO, A.Y. and ARTHUR, J.R., (1975), *Prog. Solid State Chem.*, **10**, 157

COLLINS, S., LOWE, D. and BARKER, J.R.,(1985), *J. Phys. C*, **18**, 21, L637

DAPKUS, P.D., (1984), *J. Cryst. Growth*, **68**, 345

DINGLE, R., STÖRMER, H.L., GOSSARD, A.C. and WIEGMANN, W., (1978), *Appl. Phys. Lett.*, **33**, 665

EHRENREICH, H., (1961), *J. Appl. Phys. Suppl.*, **32**, 2155

ENDERS, P., (1987), *Phys. Stat. Sol. (b)*, **139**, K113

ESAKI, L. and CHANG, L.L., (1976), *Thin Solid Films*, **36**, 285

ESAKI, L. and TSU, R.,(1970), *IBM Jl. Res. Dev.*, **14**, 61

FRIEDMAN, L., (1984), *J. Phys. C*, **17**, 3999

FRÖHLICH, H., (1937), *Proc. R. Soc.*, A160, 230

FRÖHLICH, H., (1962), *Polarons and Excitons. (Ed. Kuper and Whitfield), (Oliver and Boyd).*

GARCÍA-MOLINER, F. and SIMONS, S., (1957), *Proc. Camb. Phil. Soc.*, **53**, 848

GRADSHTEYN, I.S. and RYZHIK, I.M., (1980), *Tables of integrals, series and products, (Academic Press)*

HESS, K., (1979), *Appl. Phys. Lett.*, **35**, 7, 484

HESS, K. and IAFRATE, G.J., (1984), *Electronic Product Design*, June 1984, p71

IVANOV, I. and POLLMANN, J., (1979), *S. S. Comm.*, **32**, 869

JACOBINI, C. and REGGIANI, L., (1983), *Rev. Mod. Phys.*, **55**, 3, 645

JONES, H. and ZENER, C., (1934), *Proc. R. Soc. (London)*, **A144**, 101

KANE, E.O., (1957), *J. Phys. Chem. Solids*, **1**, 249

KEARNEY M.J. and BUTCHER P.N., (1986), *J. Phys. C*, **19**, 5429

LOBWOHL, P.A. and TSU, R., (1970) *J. Appl. Phys.*, **41**, 2664

MADELUNG, O., (1978), *Introduction to Solid State Theory*, (Springer Verlag)

MARSH, A.C. and INKSON, J.C., (1984), *J. Phys. C*, **17**, 35, 6561

MORI, S. and ANDO, T., (1980), *J. Phys. Soc. Japan*, **48**, 3, 865

MOVAGHAR, B., (1986), *Semicond. Sci. and Technol.*, **2**, 185

NAG, B.R., (1972), *Theory of Electrical Transport in Semiconductors. (Pergamon)*

OKUMURA, H., MISAWA, S., YOSHIDA, S. and GONDA, S., (1985), *Appl. Phys. Lett.*, **46**, 4, 377

ONSAGER, L., (1931), *Phys. Rev.*, **37**, 405

ONSAGER, L., (1931), *Phys. Rev.*, **38**, 2265

PALMIER, J.F. and BALLINI, Y., (1980), *J. Physique Lettres*, **41**, L539

PALMIER, J.F. and CHOMETTE, A., (1982), *J. Physique*, **43**, 381

PALMIER, J.F., Le PERSON, H., MINOT, C., CHOMETTE, A., REGRENY, A and CALECKI, D., (1985) *Superlattices and Microstructures*, **1**, 1, 67

PLOOG, K. (1980), in *Crystals: Growth, Properties and Applications, Vol 3,* (Ed H.C. Freyhardt), (Springer-Verlag)

PRICE, P.J., (1957), *IBM Jnl.*, **1**, 239

PRICE, P.J., (1958), *IBM Jnl.*, **2**, 200

RODE, D.L., (1970), *Phys. Rev. B*, **2**, 4, 1012

RODE, D.L.,(1975), *Semiconductors and Semimetals*, [*eds. Willardson, R.K. & Beer, A.C.*], vol. 10, p.15-26

SAI-HALASZ, G.A., TSU, R. and ESAKI, L., (1977), *Appl. Phys. Lett.*, **30**, 651

SAKAKI, H., CHANG, L.L., LUDEKE, R, CHANG, C.A., SAI-HALASZ, G.A. and ESAKI, L., (1977), *Appl. Phys. Lett.*, **31**, 211

SAKAKI, H., (1985), *Proc. 17th Int. Conf. on Semicond., San Francisco*, pp 1551-6

SASAKI, A., (1984), *Phys. Rev. B*, **30**, 12, 7016

SAWAKI, N.,(1986), *J. Phys. C*, **19**, 4965

SCHRÖDINGER, E., (1926), *Ann. Phys (Leipzig)*, **79**, 489

SMITH, A.C., JANAK, J.F. and ADLER, R.B.,(1967), *Electronic Conduction in Solids. (McGraw-Hill)*

STONEHAM A.M., (1975), *Theory of Defects in Solids. (Clarendon)*

STÖRMER, H.L., (1983), *Surf. Sci.*, **132**, 519

STÖRMER, H.L., DINGLE, R., GOSSARD, A.C., WEIGMANN, W. and STURGE, M.D., (1979), *S. S. Comm.*, **29**, 705

TAO, Z., and FRIEDMAN, L., (1985), *J. Phys. C*, **18**, L455

TING, D.Z.-Y. and CHANG, Yia-Chung, (1987), *Phys. Rev. B*, **36**, 8, 4359

TSUI, D.C. and LOGAN, R.A., (1979), *Appl. Phys. Lett.*, **35**, 99

VOISIN, P., (1984), in *Two-Dimensional Systems, Heterostructures and Superlattices*, (Eds. G. Bauer, F. Kuchar and H. Heinrich), (Springer-Verlag)

von KLITZING, K., (1986), *Rev. Mod. Phys.*, **58**, 519

von KLITZING, K., DORDA, G. and PEPPER, M., (1980), *Phys. Rev. Lett.*, **45**, 494

WARREN, G.J. and BUTCHER, P.N.,(1986), *J. Semicond. Sci. Technol.*, **1**, 2,133

WONG, K.B., JAROS, M., GELL, M.A. and NINNO, D., (1986), *J. Phys. C*, **19**, 53

ZIMAN, J.M., (1972), *Principles of the Theory of Solids, (C.U.P.)*